

LEVEL *II*

(1)

AD A103885

**THE EFFECT OF
INTEROCULAR CONTRAST
AND OCULAR DOMINANCE
ON THE PERCEPTION
OF MOTION-IN-DEPTH
IN 3-D DISPLAYS**

Technical Report

August 1981

DTIC
ELECTE
S SEP 8 1981 **D**
H

By: Thomas P. Plantanida, Senior Research Psychologist
Robert W. Hammon, Research Physiologist
Bioengineering Research Center

Prepared for:

Office of Naval Research
800 North Quincy Street
Arlington, Virginia 22217

Attn: Dr. John J. O'Hare, Code 455
Scientific Officer
Engineering Psychology Programs
Psychological Services Division

Contract N00014-79-C-0742

SRI Project 8899

DISTRIBUTION STATEMENT A
Approved for public release
Distribution Unlimited

SRI International
333 Ravenswood Avenue
Menlo Park, California 94025
(415) 859-6200
TWX: 910-373-2046
Telex: 334 486



81 9 04 073

SRI International



**THE EFFECT OF
INTEROCULAR CONTRAST
AND OCULAR DOMINANCE
ON THE PERCEPTION
OF MOTION-IN-DEPTH
IN 3-D DISPLAYS,**

9 Technical Report

11 Aug 1981

12/65

DTIC
ELECTE
SEP 8 1981
H
D

10 By: Thomas P. Piantanida / Senior Research Psychologist
Robert W. Hammon / Research Physiologist
Bioengineering Research Center

Prepared for:

Office of Naval Research
800 North Quincy Street
Arlington, Virginia 22217

Attn: Dr. John J. O'Hare, Code 455
Scientific Officer
Engineering Psychology Programs
Psychological Services Division

Contract/N00014-79-C-0742

SRI Project 8899

Approved:

Phillip S. Green, Director
Bioengineering Research Center

Earle D. Jones, Vice President
Advanced Development Division

410 281

REPORT DOCUMENTATION PAGE		READ INSTRUCTIONS BEFORE COMPLETING FORM	
1. REPORT NUMBER N14-0742-81C-0001 ✓	2. GOVT ACCESSION NO.	3. RECIPIENT'S CATALOG NUMBER	
4. TITLE (and Subtitle) THE EFFECT OF INTEROCULAR CONTRAST AND OCULAR DOMINANCE ON THE PERCEPTION OF MOTION-IN-DEPTH IN 3-D DISPLAYS		5. TYPE OF REPORT & PERIOD COVERED Technical Report	
7. AUTHOR(s) Thomas P. Piantanida and Robert W. Hammon		6. PERFORMING ORG. REPORT NUMBER	
9. PERFORMING ORGANIZATION NAME AND ADDRESS SRI International 333 Ravenswood Avenue Menlo Park, California 94025		8. CONTRACT OR GRANT NUMBER(s) N00014-79-C-0742	
11. CONTROLLING OFFICE NAME AND ADDRESS Engineering Psychology Programs, ONR 800 North Quincy Street, Code 455 Arlington, Virginia 22217		10. PROGRAM ELEMENT, PROJECT, TASK AREA & WORK UNIT NUMBERS	
14. MONITORING AGENCY NAME & ADDRESS (if diff. from Controlling Office)		12. REPORT DATE August 1981	13. NO. OF PAGES 71
		15. SECURITY CLASS. (of this report) Unclassified	
		15a. DECLASSIFICATION/DOWNGRADING SCHEDULE	
16. DISTRIBUTION STATEMENT (of this report) For Public Release; Distribution Unlimited			
17. DISTRIBUTION STATEMENT (of the abstract entered in Block 20, if different from report)			
18. SUPPLEMENTARY NOTES			
19. KEY WORDS (Continue on reverse side if necessary and identify by block number) Depth Perception Ocular Dominance Motion-in-Depth Eye Movements 3-D Displays Vergence Interocular Contrast Version			
20. ABSTRACT (Continue on reverse side if necessary and identify by block number) This study evaluates the maximum permissible luminance difference between stereo pairs (interocular contrast) consistent with the unambiguous perception of motion-in-depth of objects imaged on binocular 3-D displays. Objective measures (vergence eye movements) and subjective measures (observer responses) of motion-in-depth suggest (1) that the maximum interocular contrast ratio between stereo pairs should not exceed a value of about 3, (2) that the brighter of the two stereo pairs should be presented to the observer's nondominant eye, and (3) that the observer should be well trained in the use of his 3-D display to optimize his perception of motion-in-depth.			

CONTENTS

LIST OF ILLUSTRATIONS.....	3
LIST OF TABLES.....	5
I INTRODUCTION.....	7
II METHODS.....	9
A. Apparatus.....	9
1. Eyetracker.....	9
2. Stimulus Deflector.....	9
3. Display System.....	11
B. Observers.....	12
C. Procedures.....	13
III RESULTS.....	19
IV DISCUSSION.....	35
V CONCLUSIONS.....	39
REFERENCES.....	41
APPENDICES	
A Accurate Three-Dimensional Eyetracker.....	43
B Three-Dimensional Visual Stimulus Deflector.....	61

ILLUSTRATIONS

1	Schematic of Eyetracker System.....	10
2	Schematic of Stimulus Deflector.....	11
3	Schematic of Display System.....	12
4	Vergence and Version During Degradation of Stereo Pairs.....	14
5	Interocular Contrast Ratio Thresholds for the Perception of Lateral Motion of a 3.0-fL Stimulus.....	21
6	Interocular Contrast Ratio Thresholds for the Perception of Lateral Motion of a 1.5-fL Stimulus.....	23
7	Interocular Contrast Ratio Thresholds for the Perception of Motion-in-Depth of a 3.0-fL Stimulus.....	25
8	Interocular Contrast Ratio Thresholds for the Perception of Motion-in-Depth of a 1.5-fL Stimulus.....	26
9	Transition Interocular Contrast Ratios of Trained and Naive Observers for the Perception of Motion-in-Depth, Ambiguous Motion, and Lateral Motion of a 3.0-fL Stimulus.....	27
10	Transition Interocular Contrast Ratios of Trained and Naive Observers for the Perception of Motion-in-Depth, Ambiguous Motion, and Lateral Motion of a 1.5-fL Stimulus.....	28
11	Transition Interocular Contrast Ratios of the Dominant and Nondominant Eyes of a Left-Eye-Dominant Observer for the Perception of Motion-in-Depth, Ambiguous Motion, and Lateral Motion of a 1.5-fL Stimulus.....	29

12	Transition Interocular Contrast Ratios of the Dominant and Nondominant Eyes of a Right-Eye-Dominant Observer for the Perception of Motion-in-Depth, Ambiguous Motion, and Lateral Motion of a 1.5-fL Stimulus.....	30
13	Transition Interocular Contrast Ratios of the Dominant and Nondominant Eyes of a Right-Eye-Dominant Observer for the Perception of Motion-in-Depth, Ambiguous Motion, and Lateral Motion of a 3.0-fL Stimulus.....	31
14	Physiological and Subjective Measures of Observer Responses.....	32

TABLES

1	Mean (\bar{x}) and Standard Error of the Mean (SEM) of the Interocular Contrast Ratio for the Perception of Only Lateral Movement.....	20
2	Relationship Between Polarizer Angle and Interocular Contrast Ratio.....	22
3	Analysis of Differences in Interocular Contrast Ratio at Which Trained Versus Naive Observers Perceive Stimulus Moving Only Laterally.....	22
4	Mean (\bar{x}) and Standard Error of the Mean (SEM) of the Interocular Contrast Ratio for the Perception of Only Motion-In-Depth.....	24
5	Analysis of Differences in Interocular Contrast Ratio at Which Trained Versus Naive Observers Perceive Stimulus Moving Only Laterally.....	25
6	Analysis of Ocular Dominance Effects.....	28

I INTRODUCTION

Three-dimensional display systems can be divided into two categories: binocular displays and autostereoscopic displays (see Okoshi, 1976, for examples). Binocular displays present two images to the observer, but each of the observer's eyes views only one image of the stereo pair. Segregating the two images so that each eye sees only one is accomplished by a variety of techniques. Virtually every technique requires some type of device, such as the mirrors of a Wheatstone stereoscope (Wheatstone, 1838) or the prisms of a stereoscope similar to that built by Brewster in 1849 (see Brewster, 1856), between the observer's eyes and the pair of images on the display surface. Several more recently developed binocular three-dimensional display systems require that the observer wear the segregation device like spectacles. In this case, the device may consist of a pair of orthogonally oriented plane polarizers (see Butterfield, 1970, for examples), a pair of red and green or red and blue filters (see Julesz, 1971, for numerous examples), or electro-optical shutters (Roese, 1975).

Two recent developments, the helmet-mounted display system (HMD) and the heads-up display system (HUD), achieve image segregation by projecting two complete images, each of which is directed toward and seen by only one eye (cf. Hughes et al., 1973).

Autostereoscopic displays, however, require no monocular image segregation device interposed between the observer and the display but instead segregate the left- and right-eye images at the display itself. For example, in parallax panoramagrams, the left- and right-eye images can be isolated by a series of pinholes in an opaque screen that forms the front surface of the display (Sokolov, 1911), by a plate containing a series of slits (Kanolt, 1918), or by lenticular sheets (Ives, 1930). A recently developed autostereoscopic display known as a hologram segregates left- and right-eye views of the image via phase information (cf. Gabor, 1949; Leith and Upatnieks, 1964).

Autostereoscopic displays usually consist of a single viewing surface, whereas binocular displays frequently consist of two viewing surfaces. This difference could be important for our purposes. Because both the left- and right-eye images are usually present on the same viewing surface in autostereoscopic displays, the physical variables are usually very similar. For example, the luminance and chromaticity of an image region seen by the left eye are usually very similar to those seen by the right eye, and the contrasts between adjacent regions in each image are usually the same. Autostereoscopic display systems inherently produce equality of retinal image variables just as they would be produced in free-viewing situations.

With binocular display systems, however, there is no prior assurance that the retinal image variables produced by viewing the display will be equal in both eyes. For example, it is possible for the contrast, luminance, or chromaticity of the image seen by the left eye to be quite different from that seen by the right eye. We know from the work of Ogle and Groch (1956), Lit (1959), and Mitchell (1970), that static depth perception is maintained even when the difference in luminance between the stereo pairs is quite large, as long as both images of the stereo pair are above their detection threshold.

In contrast to static depth perception, dynamic depth perception does not manifest the same stability when binocular image luminances are unequal. For example, we know that even small differences in the luminance presented to each eye of a binocularly viewed moving stimulus result in the distortion of perception of lateral motion and of motion-in-depth. The Pulfrich phenomenon, in which an object moving laterally back and forth in the frontal parallel plane appears to move along an elliptical path, is caused by inequality of the luminance of the retinal images of the moving object (Lit, 1949).

From the foregoing it can be concluded that the design parameters of three-dimensional binocular displays that present objects arrayed only statically in depth need not include measures of inequality of luminance. However, a three-dimensional display designed to depict accurately the motion of objects moving in three dimensions must present to each eye images that are very similar in luminance. Unfortunately there are currently very few data suggesting the necessary degree of similarity between the luminances of the two stereo images. This study was therefore performed to examine the distortions in the perception of motion-in-depth that occur when an observer views a binocular three-dimensional display composed of left and right stereo images with different luminances. The results should define the tolerable limits of luminance inequality of stereo pairs (which we will call interocular contrast) consistent with the accurate perception of motion-in-depth of objects presented in a binocular three-dimensional display system.

II METHODS

A. Apparatus

Three major pieces of apparatus were used in this study: a binocular three-dimensional eyetracker, a pair of stimulus deflectors, and a rear-projection stimulus display system.

1. Eyetracker

The SRI three-dimensional eyetracker consisted of a left and right mirror-image pair of dual Purkinje image eyetrackers, each of which was fitted with an optometer. A right-eye dual Purkinje image eyetracker is diagrammed in Figure 1 and is described in detail in Appendix A (Crane and Steele, 1978). A brief description of the components and functions of the eyetracker follow.

Illumination for the dual Purkinje image eyetracker is provided by a solid-state spectral infrared source, shown as S_1 in Figure 1. The source illuminates the observer's eye through a system of lenses and mirrors. The collecting system images reflections of the source from the anterior surface of the observer's cornea (first Purkinje image) and from the posterior surface of the observer's lens (fourth Purkinje image) onto the surfaces of quadrant photocells P_1 and P_4 . Feedback from photocell P_1 to the servo-controlled first mirror system maintains the first Purkinje image in the center of the photocell. Likewise, feedback from photocell P_4 to the servo-controlled fourth mirror system maintains the fourth Purkinje image in the center of that photocell. The horizontal and vertical error signals from P_4 that drive the mirror system provide an accurate measure of horizontal and vertical rotations of the observer's eye.

2. Stimulus Deflector

The stimulus deflector shown in Figure 2 is described in detail in Appendix B (Crane and Clark, 1978). It consists of two unity-gain relay lens pairs that re-image the observer's eye in the plane of two mirrors that can be rotated by small high-frequency motors. The vertical deflection mirror (M_V) can be rotated about its horizontal axis, causing images to translate vertically across the observer's field of view. Likewise, rotating the horizontal deflection mirror (M_H) causes horizontal translation of images.

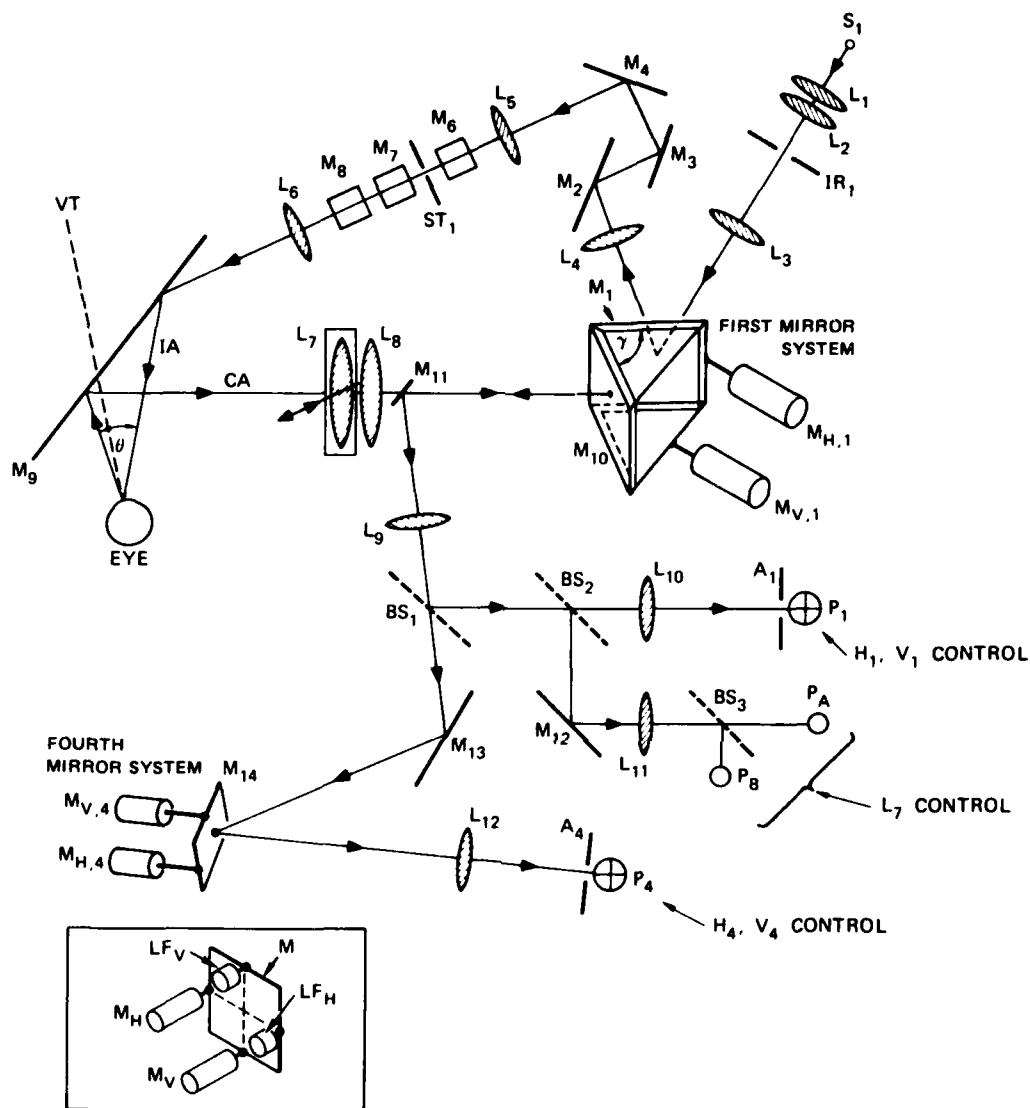


FIGURE 1 SCHEMATIC OF EYETRACKER SYSTEM

S_1 , IRLED source; IR_1 , adjustable iris conjugate with eye pupil; M_1 and M_{10} , coupled front-surface mirrors under control of motors $M_{H,1}$ and $M_{V,1}$; γ , angle between mirrors M_1 and M_{10} ; $M_2, M_3, M_4, M_6, M_7, M_8, M_{11}, M_{12}$, and M_{13} , front-surface mirrors (mirrors M_2, M_3, M_4 , and M_5 , not shown, are used in different combinations to alter the angle θ of the incoming illumination); M_{14} , front-surface mirror driven by motors $M_{V,4}$ and $M_{H,4}$; M_9 , dichroic mirror; BS_1 , 90/10 pellicle beam splitter; BS_2 and BS_3 , 50/50 beam splitters; P_1 and P_4 , quadrant photocells; A_1 and A_4 , apertures in front of P_1 and P_4 , respectively; P_A and P_B , photocells in automatic focus-detection circuit; VT , visual target; IA , input axis; CA , collecting axis; stop ST_1 , source of Purkinje image pattern; LF_H and LF_V , linear followers.

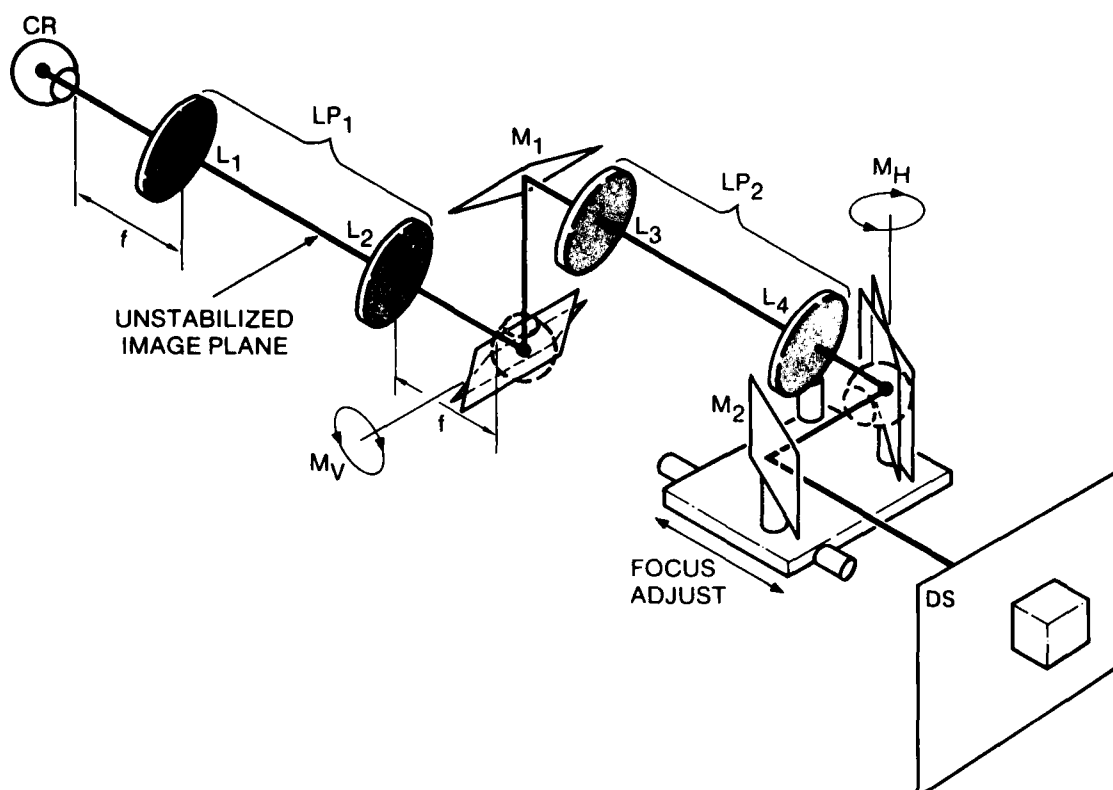


FIGURE 2 SCHEMATIC OF STIMULUS DEFLECTOR

CR, center of rotation of eye; L_1 , L_2 , L_3 , and L_4 , multiple-element camera lenses; LP, lens pair; AP, artificial pupil; DS, display screen; M_v , mirror that rotates the visual field vertically; M_h , mirror that rotates the visual field horizontally; M_1 , fixed mirror; L_4 , M_h , and mirror M_2 move in synchronism to adjust the optical distance to the display screen.

For this study, the electrical signal used to drive the horizontal mirror was a sine wave of sufficient amplitude to cause an excursion of one degree of horizontal translation peak-to-peak, with a frequency of 0.2 Hz. An inverted signal was transmitted to the companion stimulus deflector in front of the observer's other eye, resulting in antiphase horizontal translation of the images seen by each eye.

During the study presented here, the vertical deflection mirrors were fixed in position.

3. Display System

Figure 3 diagrams the display system used for rear projection of the stimuli used in this study. A Kodak Carousel 650H was used to project a pair of images from a single photographic slide. P_R is a plane polarizer that can be rotated about the ray path. P_H and P_V are orthogonally oriented plane polarizers. Front-surface mirrors M_1 and M_2 were cemented to the faces of a 90° prism that served as a beam diverter. Prisms P_1 and P_2 rotated the diverted beams 90° so that they were

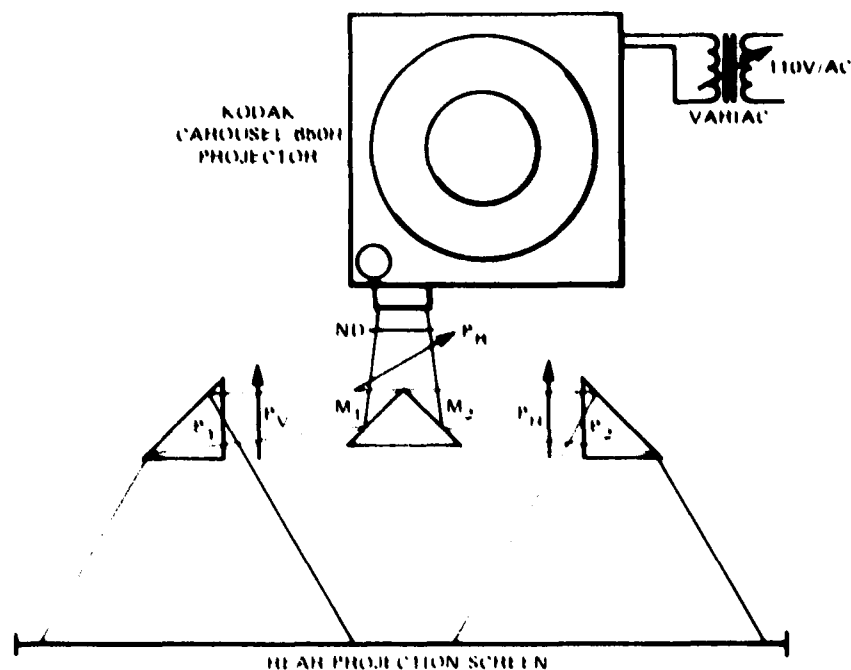


FIGURE 3. SCHEMATIC OF DISPLAY SYSTEM

ND, neutral density filter; P_R , rotatable plane polarizer; P_V , vertical plane polarizer; P_H , horizontal plane polarizer; M_1 and M_2 , front surface mirrors; P_1 and P_2 , prisms

parallel. The resultant two mirror images of the same stimulus slide were rear-projected on a translucent screen positioned 60 cm from the final element of the stimulus deflector system. Maximum luminance of the screen was controlled in two ways: by a variable transformer that varied the voltage to the project lamp and by neutral density (ND) filters that could be interposed in the beam in the plane of P_R . The maximum intensity of the two beams was balanced by inserting neutral density filters in the plane of either P_V or P_H . The relative intensities of the two beams could be varied by rotating the plane polarizer P_R . A maximum attenuation of over two log units was possible with this apparatus.

B. Observers

The co-authors served as experienced observers in this series of experiments. Naïve observers were solicited from the student population of Stanford University.

During their first visit to the laboratory, naïve observers were informed of the procedures to be followed in the study and of the hourly rate at which they would be paid for their participation. A dental impression bite bar was made for each participant. This bite bar was securely mounted on a post between the left and right eyetrackers and was adjusted vertically until the observer could see through the

stimulus deflector system. The two pads of the forehead rest were then adjusted so that the observer was maintained effortlessly in a fixed position with respect to the left and right eyetrackers. The experimenter moved each eyetracker in three dimensions until the servo mechanisms locked on the observer's first and fourth Purkinje images.

Observers were instructed to look to the upper, lower, left, and right edges of the field of view to determine whether the eyetrackers could follow each of these maximum excursions. Because of the variability in pupil size among observers, this test was performed to determine whether the margin of the pupil occluded the fourth Purkinje image during the maximum allowable horizontal or vertical excursion of the eye. The only observer for whom this presented a problem was the experimenter. The pupil size of all other observers was sufficiently large to allow tracking of the fourth Purkinje image while the observer viewed any area of the stimulus field.

Signals corresponding to the horizontal rotation of each eye were transmitted to a four-channel recorder. These signals were also used to generate a vergence/version trace on the same chart recorder by balancing their amplitude and subtracting the left signal from the right signal. Because vergence signals from the two eyes are of opposite sign, subtracting them results in an increase in the amplitude of the trace on the chart recorder. Conversely, version eye signals are of the same polarity, so subtracting one signal from the other results in a decreased trace amplitude. Because the images of the two stimuli were driven sinusoidally in antiphase, the vergence signals were also nearly sinusoidal, with the same frequency as the stimulus motion. However, version eye movements were not time-locked to the sinusoidal stimulus motions and therefore showed little sinusoidal component in their trace. Figure 4 shows signal traces during vergence and version eye movements.

Ten observers participated in this experiment, although not all of them completed each of the experimental conditions. Six were male, four female--all with the age range of 18 to 41. Observers were either emmetropic or correctable to 20/20. Each observer's "sighting ocular dominance" (see Walls, 1951, for definition) was determined by a pinhole sighting technique similar to that reported by Scherdmann (1931). Observers were asked to sight a target through a hand-held pinhole aperture in an opaque card. The results of this dominance test were recorded by an independent observer and were not revealed to the experimenter until the conclusion of the study.

C. Procedures

At the beginning of each experiment session, the observer's bite bar and forehead rests were adjusted to a comfortable position, and the eyetrackers were moved in three dimensions until each locked onto its respective Purkinje image. Where required, cylindrical lenses of appropriate dioptic power and orientation were inserted in the stimulus deflector to correct the observer's astigmatism. Spherical error, if

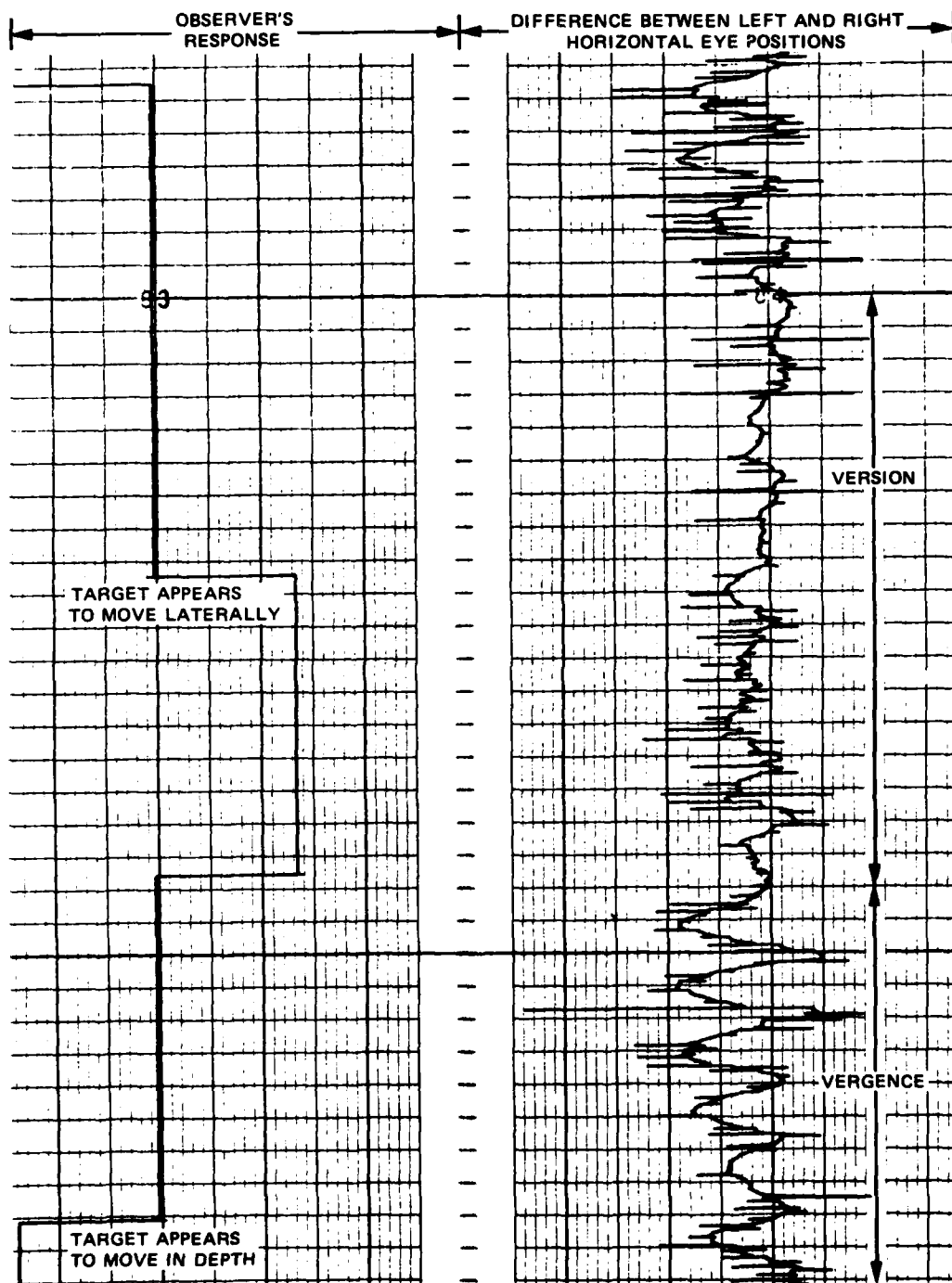


FIGURE 4 VERGENCE AND VERSION DURING DEGRADATION OF STEREO PAIRS

any, was corrected by moving the focus adjustment. A circular aperture subtending approximately ten degrees was inserted in each of the stimulus deflector systems, and the observer moved these apertures so that they appeared fused. Thus the observers viewed the binocular stimuli moving within a 10° field of view. Observers responded by activating a three-position switch to indicate when the stimulus motion appeared to be only in depth, lateral, or ambiguous (i.e., had both depth and lateral components).

At the beginning of each experimental session, observers viewed a calibration target that consisted of concentric rings surrounding a central fixation point. The target rings were spaced to correspond to 1° increments of visual angle from the central fixation point. As the subject viewed different points on the calibration target under instructions from the experimenter, the horizontal rotation signals from each eyetracker were adjusted so that a 1° rotation resulted in a fixed voltage change. The amplitude of the change was assessed from chart recorder excursions caused by the horizontal and vertical eye movements. When calibration was complete, a 1° horizontal rotation of either of the subject's eyes produced a 1-cm excursion of its own horizontal channel. The balanced horizontal signals from each eye were filtered to remove high-frequency components and were then used to drive the vergence circuit. Fine adjustments of the inputs to the vergence circuit were made with potentiometers on the vergence circuit amplifier.

To start an experimental session, a slide containing a stimulus with (nominally) 100 percent contrast was projected on the rear-projection screen. The variable polarizer was placed in approximately the 45° position, resulting in the projection of two equiluminous stimuli. The sine-wave generator used to drive the horizontal mirrors of the stimulus deflectors was turned off, and the observer varied the bias to the left and right stimulus deflectors until the fused stimulus was in the middle of his fusional range. The experimenter occluded the projection beam, inserted the stimulus slide with the appropriate contrast, and an experimental trial was initiated.

Two types of trials were conducted: one in which the observer initially saw the stimulus moving in depth and ultimately saw it moving only laterally, and the converse. Each trial that started with the stimulus moving in depth was initiated with the variable polarizer in approximately the 45° position. The experimenter slowly rotated the polarizer (P_R in Figure 3), resulting in inverse changes in the luminance of the left and right images presented on the screen. Within each type of trial, two symmetrical series were run: one that increased the luminance of the image seen by the left eye above the mean luminance, and the other that increased the luminance of the image seen by the right eye. The observer's task was to signal, by means of the three-position switch, when the stimulus no longer appeared to be moving just in depth but also seemed to be moving laterally back and forth in the field of view, and also to signal when the stimulus appeared to be moving only laterally (i.e., when there was no axial component to the perceived motion of the object).

Trials conducted to determine the interocular contrast at which the observer first saw the stimulus moving in depth were initiated with the polarizer 0° or 90° (ten trials each). The polarizer was slowly rotated toward 45° until the observer responded that the stimulus appeared to move only in depth.

During each of the trials, the signals from the eyetracker and from the vergence circuit were recorded on the chart recorder, along with the observer's response. The experimenter slowly rotated the plane polarizer and recorded the angular position at which the observer reported that the stimulus was moving only laterally. The experimenter rotated the polarizer a few degrees more in the same direction and then reversed the direction of rotation, noting the angle of the polarizer at which the observer indicated that the stimulus was again seen to move in depth. Thus for a single trial, two values were recorded: the smallest angle of rotation at which lateral motion was first perceived, and the greatest angle of rotation at which only motion-in-depth could first be seen. In each experimental session, twenty trials were run, consisting of ten trials in which the luminance of the left image was increased, and ten in which the luminance of the right image was increased.

The angular rotation of the plane polarizer was first converted to a contrast ratio between the luminances of the left and right stimuli, using Equation (1). The data were then converted to a percent interocular contrast, using Equation (2). The percent interocular contrasts at which only motion-in-depth was perceived and only lateral motion was perceived were plotted as functions both of the mean luminance of the targets and of the nominal contrast of the targets.

$$\text{Contrast ratio} = \frac{\sin^2 \theta L}{\cos^2 \theta L} \quad (1)$$

$$\text{Percent contrast} = 100(\sin^2 \theta L - \cos^2 \theta L) \quad (2)$$

where θ is the rotation of the rotatable polarizer in degrees and L is the maximum luminance of the stimulus.

Stimuli consisted of light squares subtending 4° on a side, viewed against dark surrounds. Five contrast ratios were used in this study. The actual percent contrasts of the stimuli were 37, 49, 67, 83, and 96. These contrast percentages are reported nominally here as 20, 40, 60, 80, and 100. However, when the data from this study are plotted, the slide contrasts are reported at their nominal values, but their ordinates conform to their actual percent contrast values.

Two different luminance levels of the square targets were evaluated. The mean luminance level of the targets reported here is the luminance level of the balanced targets. Consequently, at an interocular contrast ratio of one, both targets would have the same luminance,

which would be the nominal mean luminance value for this experimental series. At higher interocular contrast ratios (for example, about 1:200, the luminance level of one of the targets would be approximately twice the mean luminance level, while that of the other target would be near zero. The two luminance levels tested in this study were 1.5 and 3.0 footlamberts (fL).

III RESULTS

The major finding of this study is that most observers continue to see at least some motion-in-depth in the dichoptically presented stimuli until the interocular contrast ratio is quite high, on the order of 50:1* (which corresponds to an interocular contrast of about 96 percent). The means and standard errors of the interocular contrast ratios resulting in the perception of only lateral motion are presented in Table 1 as a function of the nominal stimulus slide contrast and the nominal stimulus luminance. The table shows the data for the trained observers (TP and RH), for the naive observers, and for all observers.

The mean interocular contrast ratios at which naive and trained observers first saw only lateral motion at a mean luminance level of 3.0 fL are plotted in Figure 5 as a function of the contrast of the stimulus slide. The error bars are the standard error of the mean. As can be seen from this figure, the interocular contrast ratios at which trained observers first saw only lateral motion of the stimuli were considerably higher than analogous contrast ratios selected by naive observers at all levels of stimulus contrast. This figure also demonstrates that not only did trained observers continue to see some motion-in-depth at a higher interocular contrast ratio than naive observers, but also that trained observers were more variable in the interocular contrast ratio at which they perceived stimulus motion only as lateral. Both the elevated interocular contrast ratio and the variability of this ratio can be explained by considering the way these ratios are generated.

The ratios are produced by rotating a polarizer in two orthogonally plane polarized beams, which produces inverse changes in luminance in the two beams. When the polarizer is near 45°, a small rotation, say 3°, results in a small change in the interocular contrast ratio. However, when the polarizer is close to the polarization axis of one of the beams (near 90°, for example), it is very nearly orthogonal to the polarization axis of the other beam. Consequently, one beam is near extinction; very small rotations of the polarizer then result in very large changes in the interocular contrast ratio. The rate of rotation of the polarizer was independent of position and was approximately the same at all angles. Table 2 shows the relationship between the polarizer angle and the interocular contrast ratio, as well as the percent contrast. Note that a 4° rotation of the polarizer between 5° and 1° results in a change of interocular contrast ratio of from 130.6 to 3,282.1 (a difference of over 1.4 log units), whereas a 5° rotation from

*Contrast ratios will henceforth be reported as a single number (e.g., 50 instead of 50:1).

Table 1

MEAN (\bar{x}) AND STANDARD ERROR OF THE MEAN (SEM) OF THE INTEROCULAR CONTRAST RATIO
FOR THE PERCEPTION OF ONLY LATERAL MOVEMENT

Subject	Luminance (fL)	Contrast Ratio											
		100		80		60		40		20			
		\bar{x}	SEM	\bar{x}	SEM	\bar{x}	SEM	\bar{x}	SEM	\bar{x}	SEM		
Trained observers	3.0	280.1	78.2	261.7	143.4	255.9	63.0	166.5	19.3	377.9	85.4		
	1.5	95.1	45.1	102.0	32.7	171.4	55.8	72.7	22.5	52.3	14.3		
Naive observers	3.0	104.8	27.3	90.2	30.3	49.0	7.6	42.4	3.9	46.2	5.5		
	1.5	32.6	4.8	56.8	10.7	34.1	6.2	31.8	6.0	29.2	5.3		
All observers	3.0	148.6	33.1	133.1	43.6	118.0	30.7	73.4	14.8	141.0	44.1		
	1.5	50.4	9.5	68.1	11.9	73.3	14.7	43.4	8.8	40.1	6.1		

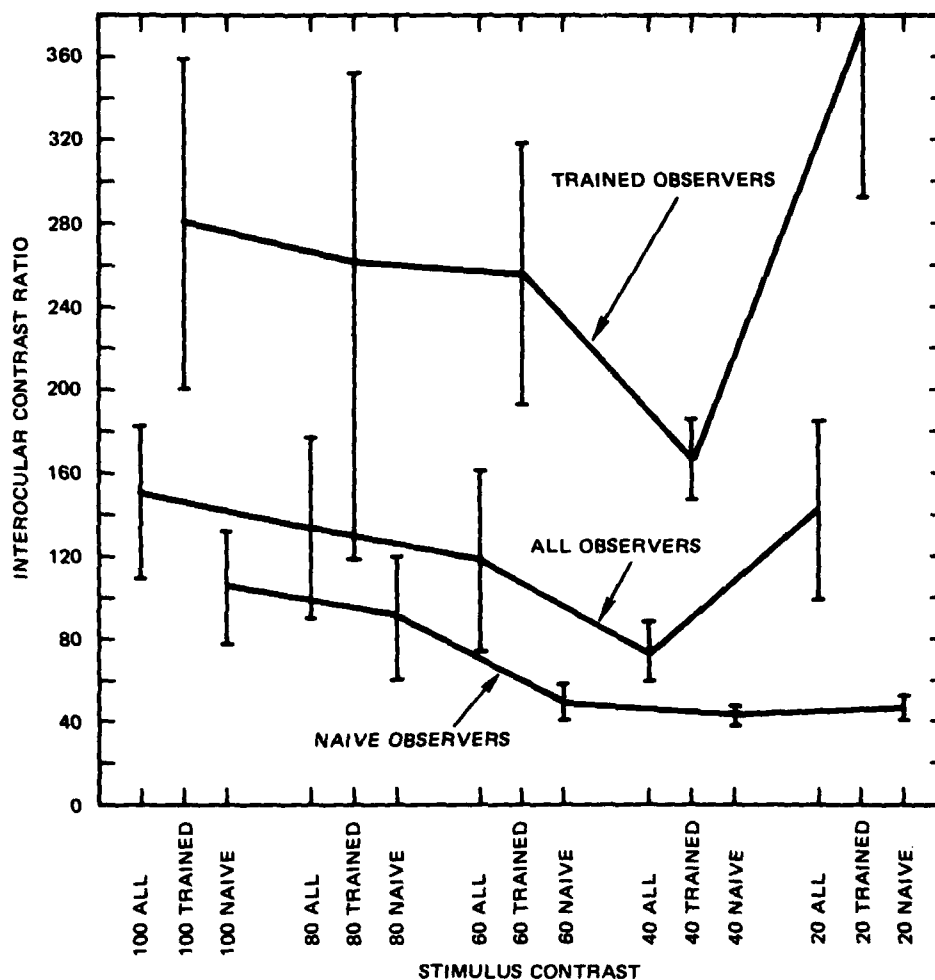


FIGURE 5 INTEROCULAR CONTRAST RATIO THRESHOLDS FOR THE PERCEPTION OF LATERAL MOTION OF A 3.0-FL STIMULUS

5° to 10° results in a change in contrast ratio of from 130.6 to 32.2 (a change in ratio of only 0.6 log units). It can be seen from Table 2 that if the angular variability of the polarizer setting for two observers is the same, but one observer has a mean polarizer setting of 5° and the other of 2°, then the observer with the mean setting of 5° will show much less variability in his interocular contrast ratio than the observer with the mean of 2°. A review of Figure 5 will show that the mean interocular contrast ratio of trained observers is higher than that of naive observers. This corresponds to a more extreme polarizer setting, with its consequent greater variability of interocular contrast ratio.

The differences between naive and experienced observers shown in Figure 5 achieved statistical significance at all nominal stimulus slide

Table 2

RELATIONSHIP BETWEEN POLARIZER ANGLE
AND INTEROCULAR CONTRAST RATIO

Polarizer Angle	Interocular Contrast Ratio	Percent Contrast
1° (89°)	3282.1	99.9
2° (88°)	820.0	99.8
5° (85°)	130.6	98.5
10° (80°)	32.2	94.0
20° (70°)	7.54	76.6
30° (60°)	3.00	50.0
40° (50°)	1.42	17.4
45° (45°)	1.00	0

contrasts. The probability of differences in interocular contrast of these magnitudes occurring by chance is less than 0.05 under any of the experimental conditions. This analysis is also shown in Table 3.

Table 3

ANALYSIS OF DIFFERENCES IN INTEROCULAR CONTRAST RATIO
AT WHICH TRAINED VERSUS NAIVE OBSERVERS
PERCEIVE STIMULUS MOVING ONLY Laterally

Luminance (fL)	Contrast Ratio									
	100		80		60		40		20	
	t	p	t	p	t	p	t	p	t	p
3.0	2.75	<0.01	1.87	<0.05	5.65	<0.005	10.01	<0.005	7.10	<0.005
1.5	4.17	<0.005	1.67	>0.05	3.95	<0.005	2.39	<0.05	1.82	<0.05

Figure 6 shows data gathered at a mean luminance of 1.5 fL. Results similar to those shown in Figure 5 (3.0 fL) are evident here. However, the mean interocular contrast ratio of the trained observers is somewhat lower than that for the same data obtained under the 3.0-fL condition. As a result, the variability of the interocular contrast ratio for these observers is also reduced.

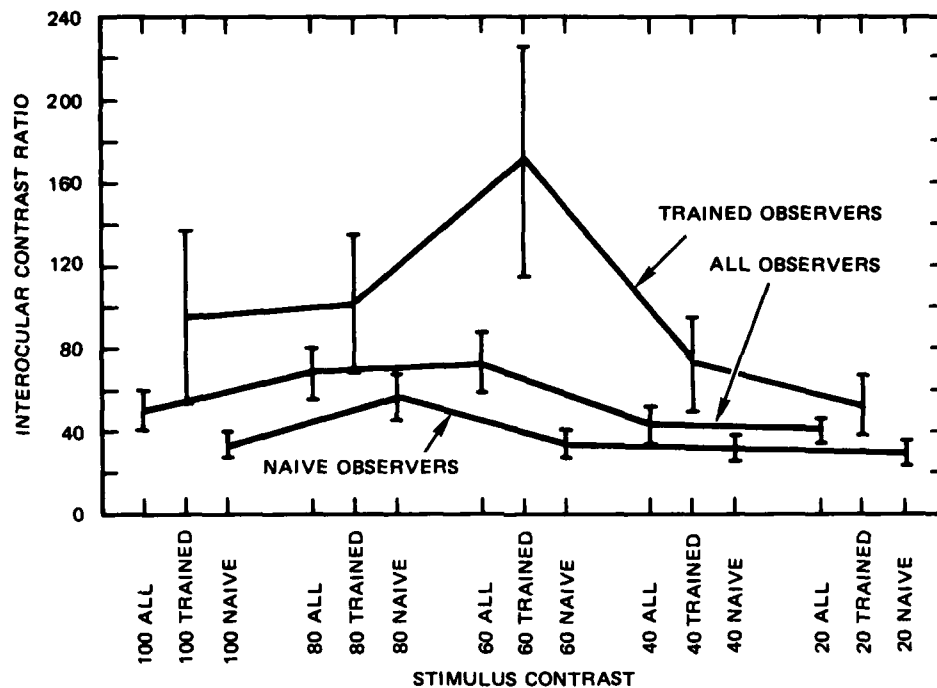


FIGURE 6 INTEROCULAR CONTRAST RATIO THRESHOLDS FOR THE PERCEPTION OF LATERAL MOTION OF A 1.5-fL STIMULUS

In Table 3, a statistical analysis of the data presented in Figure 6 reveals significant differences between the interocular contrast ratios of trained and naive observers at a luminance level of 1.5 fL for all nominal stimulus slide contrasts, except for the 80 percent contrast condition. This condition approached statistical significance ($p < 0.1$) while each of the other conditions had a probability of chance occurrence of less than 0.05.

The means and the standard error of the mean of the interocular contrast ratios at and below which observers saw the stimulus moving exclusively in depth are presented in Table 4. They are listed as a function of the nominal stimulus slide contrast and of the mean stimulus luminance. The means and standard errors of the interocular contrast ratios for the perception of exclusively motion-in-depth when the stimulus is at 3.0 fL are plotted in Figure 7 as a function of a nominal stimulus slide contrast. Note that the ordinate scale is different by a factor of ten from that used in Figures 5 and 6. This reduction was required because perception of exclusively motion-in-depth occurred only at interocular contrast ratios below about 10.

The data presented in Table 4 and Figure 7 suggest that for stimuli at a mean luminance of 3.0 fL, trained observers tend to perceive the stimulus moving exclusively in depth at higher interocular contrast ratios at most stimulus contrast levels than do naive observers. However, at this luminance level, the differences between the means of

Table 4

MEAN (\bar{x}) AND STANDARD ERROR OF THE MEAN (SEM) OF THE INTEROCULAR CONTRAST RATIO FOR THE PERCEPTION OF ONLY MOTION-IN-DEPTH

Subject	Luminance (fL)	Contrast Ratio														
		100			80			60			40			20		
		\bar{x}	SEM		\bar{x}	SEM		\bar{x}	SEM		\bar{x}	SEM		\bar{x}	SEM	
Trained observers	3.0	12.3	5.25		8.25	1.77		8.68	1.55		9.52	2.61		8.2	2.77	
	1.5	10.73	4.33		10.77	4.84		12.98	4.90		12.50	4.32		8.60	3.02	
Naive observers	3.0	9.48	1.76		7.89	1.70		5.73	0.84		6.24	1.14		5.69	0.99	
	1.5	4.86	0.78		5.17	0.92		5.10	0.65		4.01	0.54		4.31	0.49	
All observers	3.0	10.18	1.78		7.98	1.32		6.56	0.74		7.11	1.10		6.10	1.03	
	1.5	6.54	1.44		6.57	1.42		7.35	1.66		6.43	1.58		5.53	0.97	

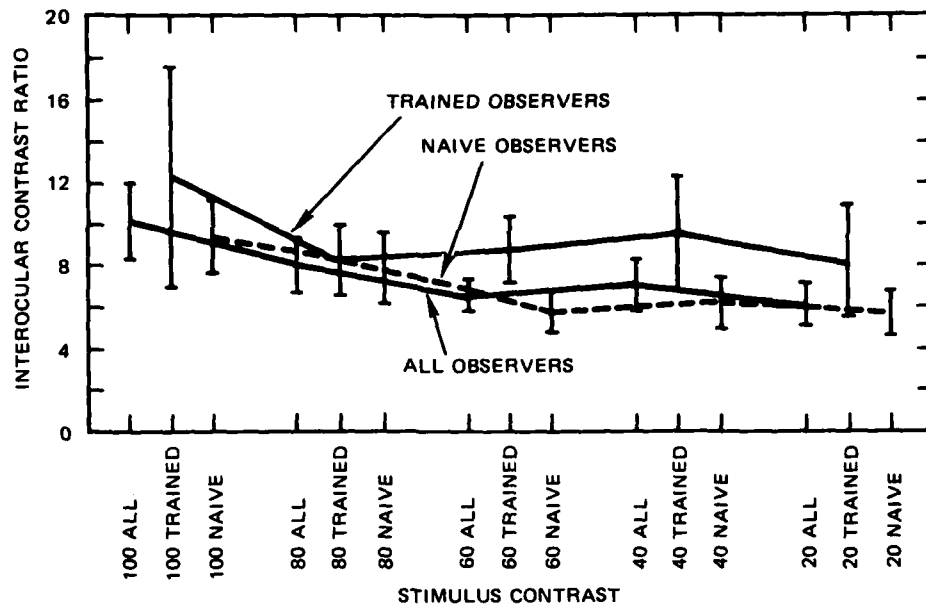


FIGURE 7 INTEROCULAR CONTRAST RATIO THRESHOLDS FOR THE PERCEPTION OF MOTION-IN-DEPTH OF A 3.0-fL STIMULUS

trained observers and naive observers achieve statistical significance only under the 60 percent nominal stimulus slide contrast condition. The results of the statistical analysis are shown in Table 5.

Table 5

ANALYSIS OF DIFFERENCES IN INTEROCULAR CONTRAST RATIO
AT WHICH TRAINED VERSUS NAIVE OBSERVERS
PERCEIVE STIMULUS MOVING ONLY Laterally

Luminance (fL)	Contrast Ratio									
	100		80		60		40		20	
	t	p	t	p	t	p	t	p	t	p
3.0	0.67	>0.05	0.11	>0.05	1.99	<0.05	1.37	>0.05	1.12	>0.05
1.5	2.06	<0.05	1.69	>0.05	2.55	<0.05	2.95	<0.01	2.09	<0.05

Differences between the mean interocular contrast at which trained observers and naive observers saw the stimulus moving exclusively in depth was even greater under the 1.5-fL condition. These data are presented in Figure 8. This figure shows that trained observers tended

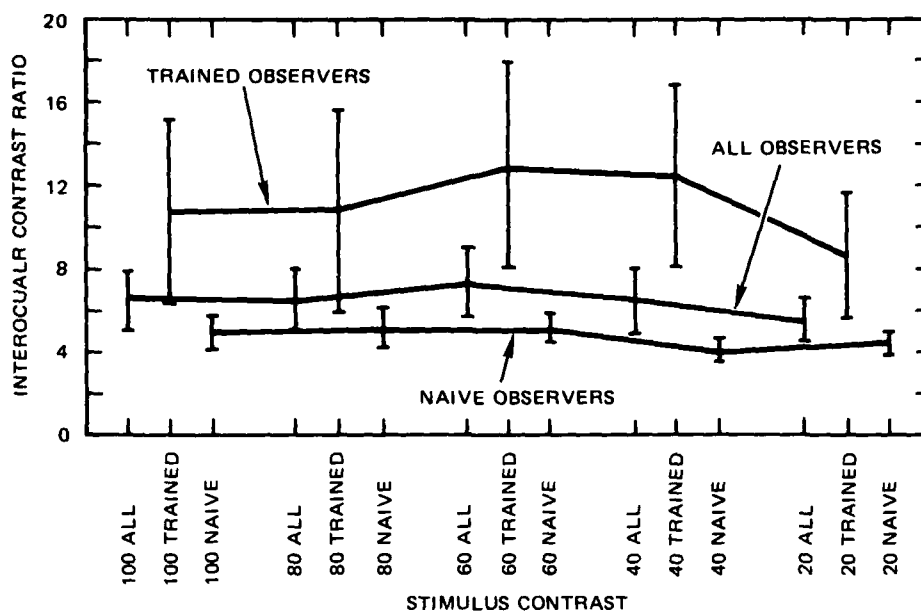


FIGURE 8 INTEROCULAR CONTRAST RATIO THRESHOLDS FOR THE PERCEPTION OF MOTION-IN-DEPTH OF A 1.5-FL STIMULUS

to continue to see the stimulus moving exclusively in depth when the interocular contrast ratio was higher than that which resulted in the naive observers' perceiving ambiguous motion of the stimulus (i.e., some lateral motion). As shown in Table 5, these differences are statistically significant at the 0.05 level except for the 80 percent nominal stimulus slide contrast condition. The t value associated with the 80 percent contrast condition corresponds to a probability of less than 0.1 that the difference between the mean of the trained observers and the mean of the naive observers was due to chance alone.

The mean interocular contrast ratios at which trained observers and naive observers first experienced either only lateral motion or only motion-in-depth are plotted in Figure 9 as a function of the nominal stimulus slide contrast for a stimulus of 3.0 fL. The isoperceptual contours define five regions in this two-dimensional space. The extreme left-hand region of the figure is a region of very low interocular contrast ratios wherein all observers saw the stimulus moving only in depth. It is bounded on the right by a contour joining the mean interocular contrast ratios above which naive observers no longer saw the stimulus moving exclusively in depth. Next is a region of interocular contrast ratios at which trained observers continued to see the stimulus moving only in depth, but naive observers saw some lateral motion to the stimulus as well. This region is bounded on the right by an isoperceptual contour at which even trained observers no longer saw the stimulus moving exclusively in depth. The next region is one in which all observers saw the stimulus moving both laterally and in depth. In the region next to it which commences at an interocular contrast ratio of

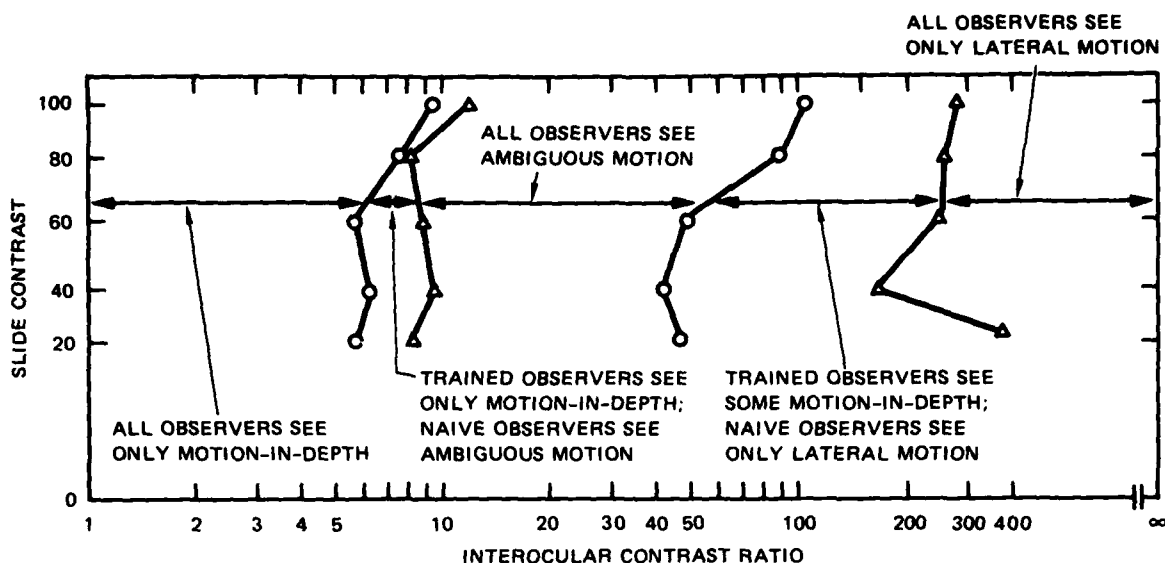


FIGURE 9 TRANSITION INTEROCULAR CONTRAST RATIOS OF TRAINED AND NAIVE OBSERVERS FOR THE PERCEPTION OF MOTION-IN-DEPTH, AMBIGUOUS MOTION, AND LATERAL MOTION OF A 3.0-fL STIMULUS

approximately 50, trained observers continued to see some motion-in-depth of the stimulus, but naive observers saw the stimulus moving only laterally. Finally, there is a region above interocular contrast ratios of approximately 200 in which all observers saw the stimulus moving only laterally.

Figure 10 shows analogous data for a stimulus presented at 1.5 fL. The same five regions observed in Figure 9 can be seen here as well. Furthermore, there is a larger difference in the mean interocular contrast at which trained observers and naive observers saw motion-in-depth only under the 1.5-fL condition than there was under the 3.0-fL condition. This can be attributed mainly to a lowering of the interocular contrast at which naive observers first saw only motion-in-depth, although there is a suggestion of an elevation of the interocular contrast ratios at which trained observers first perceived only motion-in-depth. The region of ambiguous motion is much smaller here than in the previous figure; this is mainly attributable to a shift toward lower values of the interocular contrast ratio at which naive observers first saw only lateral motion.

Early in this study it became apparent that the interocular contrast ratio at which the previously described boundary conditions occurred varied, depending on whether the luminance was greater in the observer's dominant or nondominant eye. Thus the data have been analyzed for the effect of ocular dominance.

To perform the analysis, data were collapsed over the nominal stimulus slide contrast dimension and segregated according to whether the luminance was lower in the observer's dominant or nondominant eye.

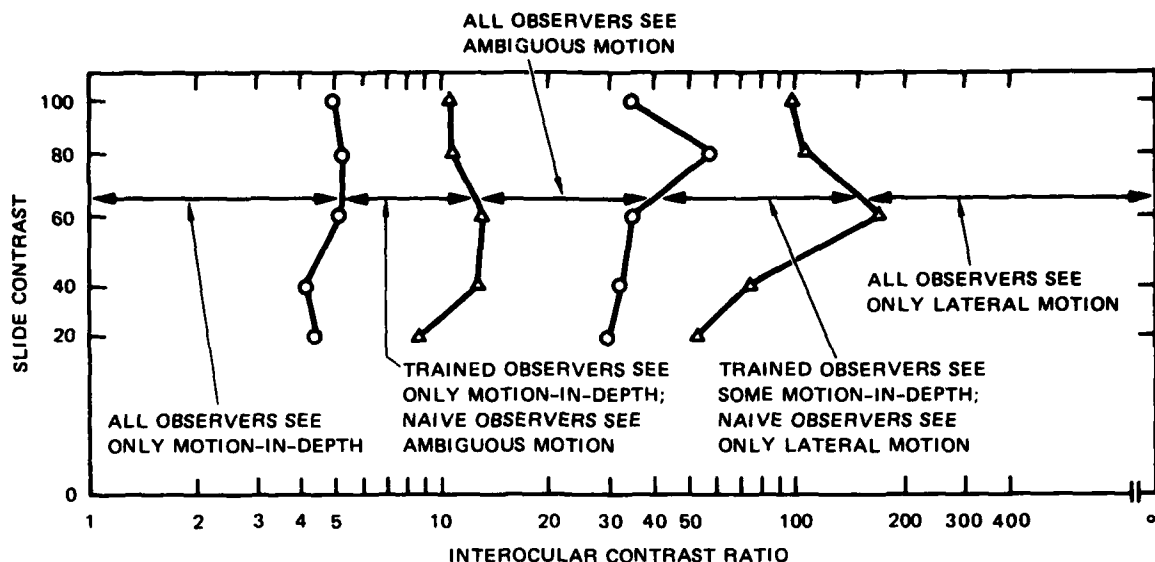


FIGURE 10 TRANSITION INTEROCULAR CONTRAST RATIOS OF TRAINED AND NAIVE OBSERVERS FOR THE PERCEPTION OF MOTION-IN-DEPTH, AMBIGUOUS MOTION, AND LATERAL MOTION OF A 1.5-fL STIMULUS

(During each experimental session, half the trials involved decreased luminance of the monocular stimulus seen by the observer's dominant eye; the other half involved decreased luminance of the stimulus seen by the observer's nondominant eye.) The results of the analysis are shown in Table 6. In the upper part of the table, the effect of ocular dominance on the perception of lateral motion only is significant at the 0.05

Table 6

ANALYSIS OF OCULAR DOMINANCE EFFECTS

Type of Motion	Luminance (fL)	Eye	Interocular Contrast			
			\bar{x}	δ	t	p
Lateral	3.0	Dominant	124.04	115.06	0.117	>0.4
		Nondominant	120.42	158.05		
	1.5	Dominant	43.80	46.40	1.78	<0.05
		Nondominant	64.48	53.38		
Depth	3.0	Dominant	6.48	3.88	2.49	<0.01
		Nondominant	9.29	5.65		
	1.5	Dominant	4.90	3.80	2.66	<0.01
		Nondominant	8.12	6.17		

level for the 1.5-fL condition but is not statistically significant for the 3.0-fL condition. Ocular dominance affects the perception of only motion-in-depth under both the 3.0-fL and 1.5-fL conditions. The effect of ocular dominance is significant under both of these conditions at the 0.01 level.

To demonstrate what this means in terms of an observer's perception of binocular stimuli when the luminance of one stimulus has been diminished in his dominant or nondominant eye, figures similar to Figures 9 and 10 have been prepared. Figure 11 shows data obtained from a left-eye-dominant observer when the stimulus had a mean luminance of 1.5 fL. On the left in the figure are two curves that show the interocular contrast ratio at and below which the observer saw the stimulus moving only in depth. The leftmost curve, which connects the circles, shows the interocular contrast ratio at which the observer first saw only motion-in-depth when the luminance of the stimulus was reduced in his nondominant eye and increased in his dominant eye. The curve that connects the triangles shows the interocular contrast ratios below which the observer saw the stimulus moving only in depth when the luminance of the stimulus was reduced in his dominant eye and increased in his nondominant eye. Between these two curves is a region of interocular contrast ratios where, if the luminance is lower in the observer's dominant eye, he will continue to see the stimulus moving in depth, but if the luminance is lower in his nondominant eye he will see the stimulus moving ambiguously. On the right side of the figure are analogous curves showing the interocular contrast ratios at and above which the observer saw the stimulus moving only laterally. The two curves, one connecting the

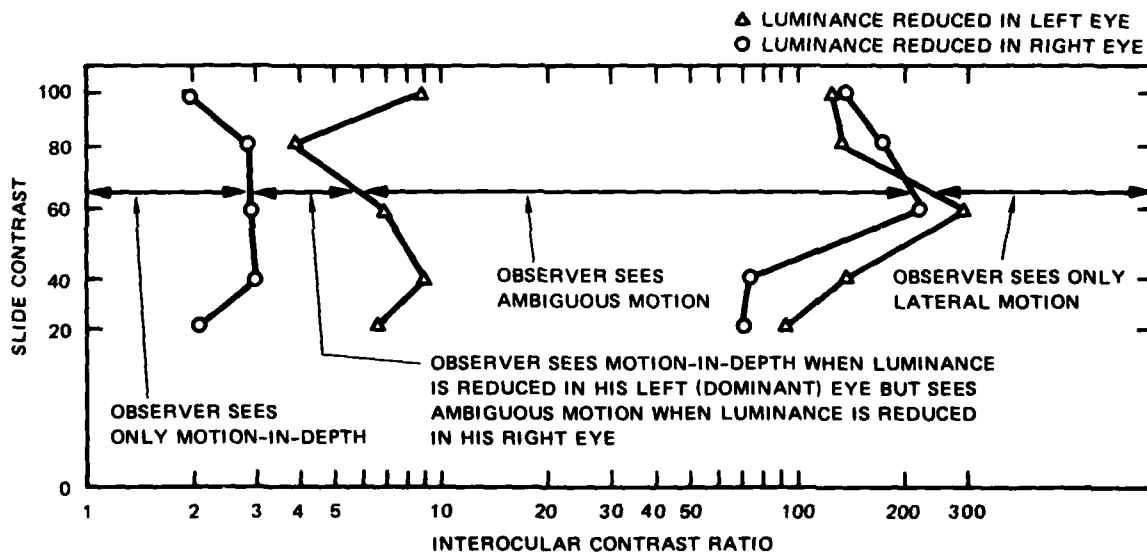


FIGURE 11 TRANSITION INTEROCULAR CONTRAST RATIOS OF THE DOMINANT AND NONDOMINANT EYES OF A LEFT-EYE-DOMINANT OBSERVER FOR THE PERCEPTION OF MOTION-IN-DEPTH, AMBIGUOUS MOTION, AND LATERAL MOTION OF A 1.5-fL STIMULUS

triangles (representing the condition in which the luminance was reduced in the dominant eye) and the other connecting the circles (the condition in which the luminance was reduced in the observer's nondominant eye) cross each other and therefore do not describe a consistent region of difference in perception attributable to ocular dominance.

The data shown in Figure 12 were obtained from a right-eye-dominant observer when the stimulus had a mean luminance of 1.5 fL. The same four curves described in the previous figure are also shown here. In this case, however, the two curves on the right show the differences in interocular contrast ratios at and above which the observer saw the stimulus moving only laterally when the luminance was reduced in his nondominant eye (circles) and when the luminance was reduced in his dominant (right) eye (triangles). This difference in lateral motion perception attributable to ocular dominance is consistent with the analysis shown in Table 6.

The two lines on the left in Figure 12 describe a region similar to that seen on the left in Figure 11, in which this right-eye-dominant observer continued to see only motion-in-depth of the stimulus at some interocular contrast ratios when the luminance was reduced in his dominant eye, but not when it was reduced in his nondominant eye to produce a corresponding interocular contrast ratio. For this observer, the region is small, but the displacement of the curves with respect to each other is consistent with right-eye dominance.

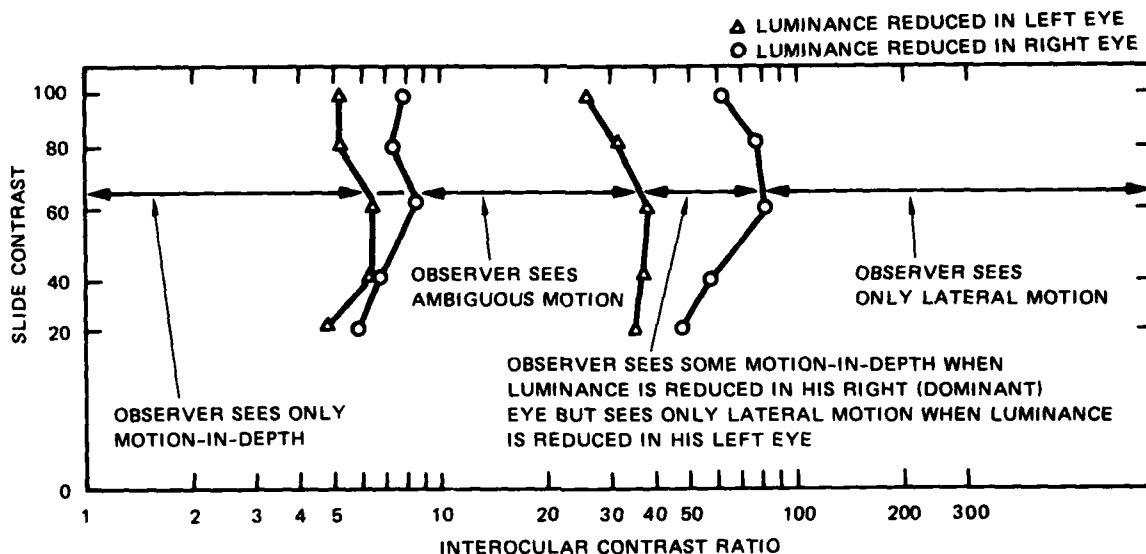


FIGURE 12 TRANSITION INTEROCULAR CONTRAST RATIOS OF THE DOMINANT AND NONDOMINANT EYES OF A RIGHT-EYE-DOMINANT OBSERVER FOR THE PERCEPTION OF MOTION-IN-DEPTH, AMBIGUOUS MOTION, AND LATERAL MOTION OF A 1.5-fL STIMULUS

The data shown in Figure 13 are also from a right-eye-dominant observer. These data were obtained at a mean luminance level of 3.0 fL. The two curves on the left show that when the interocular contrast ratio

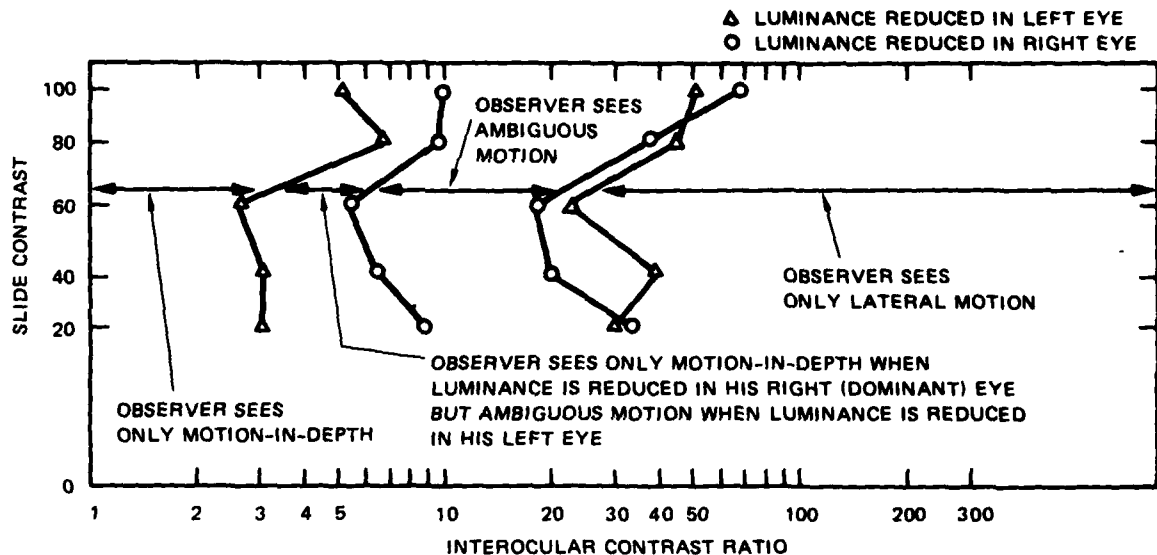


FIGURE 13 TRANSITION INTEROCULAR CONTRAST RATIOS OF THE DOMINANT AND NONDOMINANT EYES OF A RIGHT-EYE-DOMINANT OBSERVER FOR THE PERCEPTION OF MOTION IN-DEPTH, AMBIGUOUS MOTION, AND LATERAL MOTION OF A 3.0-fL STIMULUS

was produced by reducing the luminance in the observer's nondominant (left) eye, the perception of only motion-in-depth was lost at a lower interocular contrast ratio than when the luminance of the target was reduced in his dominant eye. A comparison of the two curves on the left of Figure 13 with those in Figure 11 will reveal that the position of the left-eye and right-eye curves are inverted in these two figures. This is just what would be expected from the difference in ocular dominance of the two observers who generated these sets of data.

Throughout this study, the horizontal eye movements of each observer were recorded during experimental sessions. Figure 14 shows the eye movement records obtained during a session in which a naive right-eye-dominant observer viewed an 80 percent contrast stimulus at a mean luminance level of 3.0 fL. This record was obtained during a series of trials that determined the interocular contrast ratio at which this observer first perceived the stimulus moving only laterally when the luminance of the stimulus seen by his dominant (right) eye was reduced.

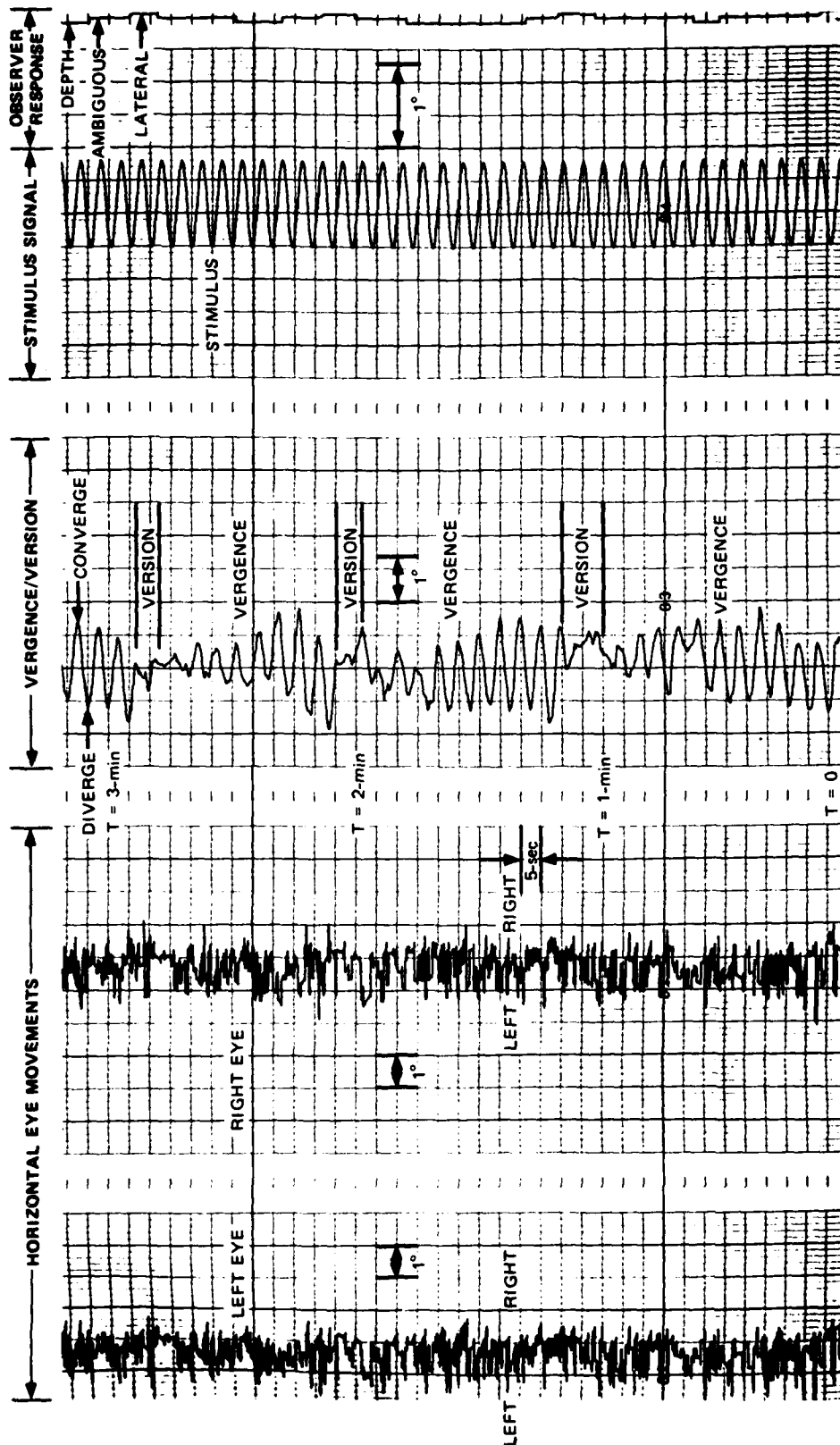


FIGURE 14 PHYSIOLOGICAL AND SUBJECTIVE MEASURES OF OBSERVER RESPONSES

The two leftmost traces in this figure show the observer's left and right eye movements during approximately three minutes of the experimental session. Notice that both eyes made numerous saccades during this time, so that it would have been impossible to determine by visual inspection whether the observer was making vergence eye movements or version eye movements. Fortunately, it was not necessary to make these judgments by visual inspection, as the middle trace in the figure reveals.

The middle trace is the difference of the right and left horizontal eye-movement signals from which the high-frequency components have been filtered. The result is a trace that is approximately sinusoidal during vergence eye movements and aperiodic during version movements. Compare the vergence signal to a stimulus signal immediately to its right. Notice that during periods when the observer made vergence movements the trace is in phase with the stimulus trace, but when the observer made version movements the phase relationship is lost.

The rightmost trace in Figure 14 is an analog of the observer's response. A rightward movement of the trace indicates that the observer is signaling perception of the stimulus moving only laterally. When the trace is in the center, the observer is signaling that the perceived motion of the stimulus is neither only lateral nor only in depth. Leftward movement of the trace indicates that the observer is perceiving the stimulus moving only in depth. A comparison of the vergence trace with the observer's response trace indicates that there is good agreement between the physiological response and the subjective response. During periods when the vergence signal is sinusoidal and of large amplitude, the observer is indicating that he is seeing the stimulus moving only in depth. As the amplitude of the vergence signal diminishes because of an increase in the interocular contrast of the stimulus, the observer indicates that the stimulus appears to be moving ambiguously. Finally, when the vergence records indicate that the observer is making exclusively version movements, the response record indicates that he is perceiving the stimulus moving only laterally. Of course, correspondence between the vergence record and the response record is not perfect because of such factors as hysteresis in the stereopsis mechanism and the need for the observer to perceive the motion of the stimulus for some finite time before deciding what that motion is. Nonetheless, the degree of correspondence is quite good.

IV DISCUSSION

The results of this study suggest that the human stereopsis mechanism is quite tolerant of differences in the luminance of stereo pairs. When the luminance of one of a pair of stereo images of an object moving in depth was reduced while the luminance of its partner was increased, most observers continued to perceive at least some motion-in-depth of the object until the interocular contrast ratio was about 30. (This corresponds to a contrast of about 93.5 percent.) These figures represent the lowest interocular contrast at which our observers began to see the stimulus moving only laterally (i.e., the luminance of one of the binocular stimuli was just below the threshold for the perception of motion-in-depth). The data were obtained under the least favorable viewing conditions--when the mean luminance of the stimulus was only 1.5 fL and the contrast of the stimulus image was only 20 percent. Under slightly improved conditions (for example, at 3.0 fL and at a stimulus contrast greater than about 60 percent), the mean interocular contrast ratio at which any of our observers began to see the stimulus moving exclusively laterally had reached 100. (This corresponds to an interocular contrast of 98 percent).

The results cited above were obtained from our naive observers. Trained observers, however, tended to be even more tolerant of luminance differences between the stereo images. Even under the worst stimulus conditions presented in this study (mean stimulus luminance of 1.5 fL and stimulus contrast of 20 percent), trained observers continued to see at least some motion-in-depth of the stimulus until the interocular contrast ratio reached about 50, corresponding to an interocular contrast of 96 percent. Even at this low luminance level, if the contrast of the stimulus was increased, say to at least 80 percent, then trained observers would tolerate an interocular contrast ratio of approximately 100 before completely losing any perception of motion-in-depth. At higher mean luminance levels, trained observers did even better. The lowest mean interocular contrast ratio at which they failed to perceive at least some motion-in-depth of the stimulus object was 160, which corresponds to 98.8 percent interocular contrast. More typically, interocular contrast ratios above 250 were required to eliminate some residual perception of motion-in-depth of the stimulus in these observers.

A review of the curves in Figures 5 and 6 suggests that the differences in the interocular contrast ratios at which naive and trained observers no longer saw any motion-in-depth of the stimulus are reduced under the 1.5-fL conditions relative to those of the 3.0-fL conditions. Under the 3.0-fL conditions shown in Figure 5, the interocular contrast ratios of naive and trained observers differ by approximately a factor of four. In Figure 6, however, the difference in interocular contrast

ratios between trained and naive observers is closer to a factor of two (especially if the average value at a nominal stimulus slide contrast value of 60 is eliminated). These data suggest that the parameter of mean stimulus luminance requires further examination.

There is also some suggestion in the data evident in Figure 5 that, at least at the 3.0-fL level of the stimulus, naive observers tend to perceive the stimulus as moving laterally at lower interocular contrast ratios when the stimuli were presented at lower contrasts. Thus when the stimulus had a contrast of 20 percent or 40 percent, naive observers started to see the stimulus moving only laterally at an interocular contrast ratio below 50. When the stimulus contrast was higher, these same observers could tolerate an interocular contrast ratio of between 50 and 100 before seeing the stimulus moving only laterally. The data obtained from trained observers were too variable to permit meaningful comparison.

That fact that some perception of motion-in-depth remains at high interocular contrast ratios should not be construed to mean that interocular contrast is an unimportant variable of binocular three-dimensional visual displays. The data imply only that some residual perception of motion-in-depth is retained even at relatively high interocular contrast ratios but say nothing about the fidelity of motion perception. At and near the interocular contrast ratios at which this residual perception of motion-in-depth is finally lost, the fidelity of perceived motion is quite low; the observers see the stimulus moving both laterally and in depth. The data that are considerably more informative about the fidelity of image motion are found at the observer's threshold for detecting only motion-in-depth. This threshold, as described in Figures 9 and 10, forms the boundary between the observer's perception of the stimulus object as moving ambiguously (i.e., with both lateral and axial components) and his perception of the object as moving only in depth.

The perception of only motion-in-depth occurs exclusively at very low interocular contrast ratios. Although the human stereopsis mechanism may continue to produce a perception of motion-in-depth when the interocular contrast ratio is quite high, to be able to perceive faithfully an object moving only in depth, the luminance of that object's binocular images must be matched fairly closely.

Once again, however, there is a difference between the interocular contrast ratio at which trained and naive observers will see the stimulus object moving only in depth. For trained observers, the transition from the perception of ambiguous motion occurs at interocular contrast ratios of between 10 and 13 at 1.5 fL and between 8 and 13 for stimuli with a mean luminance of 3.0 fL. These can be compared to interocular contrast ratios between 4 and 5 for naive observers viewing the stimulus at 1.5 fL and to interocular contrast ratios of from 5 to 10 for the same observers viewing the stimulus at a mean luminance level of 3.0 fL. There is also some suggestion that at lower nominal stimulus slide contrasts naive observers perceive the stimulus as moving

ambiguously at lower interocular contrast ratios than they do when the stimulus is of higher contrast. For example, at a mean luminance level of 3.0 fL and a nominal stimulus slide contrast of 20 percent, the transition from ambiguous motion to the perception of motion only in depth occurred at an interocular contrast ratio of approximately 6. This same transition occurred at an interocular contrast ratio closer to 10 when the stimulus had a nominal contrast of 100 percent. (These data were presented in Figure 7.) There is some suggestion that the same trend may occur among trained observers, but the variability of their data is too great to allow an accurate comparison to be made.

Generally, the transitions from the perception of only motion-in-depth to ambiguous motion and from ambiguous motion to the perception of only lateral motion occurred at higher interocular contrast ratios in trained observers than they did in naive observers. These results imply that trained observers are more likely to observe the stimulus as moving in depth under a given stimulus condition than are naive observers. Such results may be attributable to perceptual set. Both trained observers in this study were experienced in making critical visual psychophysical judgments and had spent many hours in experiments in which it was beneficial for them to suppress monocular images. The difference in variability of the data for naive and trained observers also suggests that the criterion adopted by trained observers was more variable than that adopted by naive observers. This increased variability would be consistent with conscious effort on the part of the trained observers to suppress diplopia. The success of the suppression could vary with a variety of observer factors such as motivation and fatigue as well as with stimulus factors such as luminance level. Generally, the data indicate that the differences between trained and naive observers were greater under the reduced luminance conditions that favor successful suppression of monocular images than under the elevated luminance conditions.

One of the more striking findings of this study was that, depending upon whether the higher luminance stimulus was presented to an observer's dominant or nondominant eye, the observer might see the stimulus moving only in depth or ambiguously. Furthermore, at some interocular contrast ratios, ocular dominance also determines whether an observer perceives the stimulus moving ambiguously or moving only laterally. These findings are similar in concept to those of Miles (1953), who reported that ocular dominance affected the brightness of two stimuli of equal luminance and that this brightness difference influenced the perceived relative depth of the two stimuli.

A review of Table 6 reveals that when the stimulus is at a mean luminance level of 3.0 fL, ocular dominance seems not to affect the interocular contrast ratio at which the transition from the perception of ambiguous motion to only lateral motion occurs. This is evident in Figure 13 from the proximity of the isoperceptual contours for the transition from ambiguous motion to the perception of only lateral motion

under the conditions in which the luminance of the stimulus was reduced in the left eye and in the right eye, respectively, and by the fact that these two isoperceptual contours cross each other at two points.

Ocular dominance does affect to a statistically significant extent the transition from the perception of ambiguous motion to the perception of only lateral motion when the mean luminance of the stimulus is 1.5 fL. Table 6 shows that, even though variability of the data is high, the mean interocular contrast ratio at which the transition from perception of ambiguous motion to only lateral motion perception occurs is significantly higher when the luminance of the stereo image is reduced in the dominant eye than when it is reduced in the nondominant eye.

The effect of ocular dominance can be likened to a difference in gain between the two monocular inputs to stereopsis. If the stereopsis mechanism functions best when the signals from both eyes are equal, but the same input signal to both eyes is amplified more by the dominant eye, then a reduction in the input to the nondominant eye creates greater inequality of the signals to the stereopsis mechanism, while a reduction in the luminance in the dominant eye results in greater equality of the two signals.

This crude analogy seems to hold for the transition from the perception of ambiguous motion to the perception of exclusively motion-in-depth under conditions in which observers view stimuli at a luminance level of 1.5 fL and 3.0 fL. Under each of these conditions observers tolerate much higher interocular contrast ratios while maintaining the perception of only motion-in-depth when the luminance of the stimulus viewed by the dominant eye is reduced than when the stimulus viewed by the nondominant eye is reduced. Differences attributable to ocular dominance are highly significant at both mean luminance levels. Under the 3.0-fL condition, the 50 percent increase in the interocular contrast ratio at which the transition occurs from ambiguous motion to only motion-in-depth can be attributed to ocular dominance. Likewise, under the 1.5-fL condition, a 65 percent increase in the allowable interocular contrast is produced by reducing the luminance of the stimulus seen by the observer's dominant eye relative to that seen by his nondominant eye. In addition to their statistical significance, these results have a practical significance: they suggest that for stereo displays having a mismatch in luminance of up to approximately 50 percent, the effect of this mismatch can be overcome by presenting the stereo image with the greater luminance to the observer's nondominant eye.

V CONCLUSIONS

The results of this study suggest that an evaluation of binocular three-dimensional display systems needs to include not only display variables but also variables influencing the interaction of observer and display. Specifically, for a display to produce the unambiguous perception of motion-in-depth among virtually all observers, it should produce interocular contrast ratios no greater than about 3 at the lowest luminance contrast it would normally present. Furthermore, binocular three-dimensional display systems should ideally be tailored to the individual observer's ocular dominance; the stereo image with the lower mean luminance should be presented to the observer's dominant eye. Finally, the data suggest that the observer should be trained to use his 3-D display system optimally.

REFERENCES

- Brewster, D., 1856: The Stereoscope, John Murray, London.
- Butterfield, J.F., 1970: "Three-Dimensional Television," Proc. 15th Annual SPIE Symp., pp. 3-9.
- Crane, H.D., and M.R. Clark, 1978: "Three-Dimensional Visual Stimulus Deflector," Applied Optics, Vol. 17, pp. 706-714.
- Crane, H.D., and C.M. Steele, 1978: "Accurate Three-Dimensional Eyetracker," Applied Optics, Vol. 17, pp. 691-705.
- Gabor, D., 1949: "Microscopy by Reconstructed Wavefronts," Proc. Phys. Soc., Vol. A194, pp. 454-487.
- Hughes, R.J., L. Chason, and J.C.H. Schwank, 1973: "Psychological Considerations in the Design of Helmet-Mounted Displays and Sights: Overview and Annotated Bibliography," Final Report, AMRL-TR-73-16, Aerospace Medical Research Lab, Wright-Patterson AFB, Ohio.
- Ives, H.E., 1930: "Parallax Panoramagrams for Viewing by Reflected Light," J. Opt. Soc. Am., Vol. 20, pp. 585-592.
- Julesz, B., 1971: Foundations of Cyclopean Perception, The University of Chicago Press, Ltd., London.
- Kanolt, C.W., 1918: U.S. Patent 1,260,682.
- Leith, E.N., and J. Upatnieks, 1964: "Wavefront Reconstruction with Diffrused Illumination and Three-Dimensional Objects," J. Opt. Soc. Am., Vol. 54, pp. 1295-1301.
- Lit, A., 1949: "The Magnitude of the Pulfrich Stereophenomenon as a Function of Binocular Differences of Intensity at Various Levels of Illumination," Am. J. Psychol., Vol. 62, pp. 159-181.
- Lit, A., 1959: "Depth-Discrimination Thresholds as a Function of Binocular Differences of Retinal Illuminance at Scotopic and Photopic Levels," J. Opt. Soc. Am., Vol. 49, pp. 746-752.
- Miles, P.W., 1953: "Anomalous Binocular Depth Perception due to Unequal Image Brightness," AMA Arch. Ophthalmol., Vol. 50, pp. 475-478.
- Mitchell, D., 1970: "Properties of Stimuli Eliciting Vergence Eye Movements and Stereopsis," Vision Res., Vol. 12, pp. 1241-1251.

Ogle, K.N., and J. Groch, 1956: "Stereopsis and Unequal Luminosities of the Images in the Two Eyes," AMA Arch. Ophthalmol., Vol. 56, pp. 878-895.

Okoshi, T., 1976: Three-Dimensional Imaging Techniques, Academic Press, New York and London.

Roose, J.A., 1975: "Stereoscopic Viewer Attachment," Patent application PAT-APPL-626-403.

Scherdemann, N.V., 1931: "A Simple Test for Ocular Dominance," Am. J. Psychol., Vol. 43, p. 126.

Sokolov, A.P., 1911: Autostereoscopy and Integral Photography by Professor Lippmann's Method, Izd. MGU Moscow State University Press.

Walls, G.L., 1951: "A Theory of Ocular Dominance," AMA Arch. Ophthalmol., Vol. 45, pp. 387-412.

Wheatstone, C., 1838: "On Some Remarkable, but Hitherto Unobserved Phenomena of Binocular Vision," Phil. Trans. Roy. Soc. (London), Vol. 128, pp. 371-394.

Appendix A

ACCURATE THREE-DIMENSIONAL EYETRACKER

Reprinted from Applied Optics, Vol. 17, No. 5, pp. 691-705 (1 March 1978)

Accurate three-dimensional eyetracker

H. D. Crane and C. M. Steele

A combined optometer and eyetracking instrument has been developed to measure both the dynamic refractive power and the direction of gaze of the same eye. In effect, this instrument measures, as a function of time, the point in 3-D space on which the eye is fixated. Nothing is attached to the subject (patient), who is easily aligned in the device. The measuring wavelength is in the near ir and is invisible. The usable field of the instrument is greater than 20° ; the horizontal and vertical directions of gaze are measured with a noise level and repeatability of about 1 min of arc. The range of the optometer is approximately -4 to $+12$ diopters; refractive power is measured to about 0.1 diopter. Two instruments may be aligned side by side for tracking both eyes simultaneously. Three-dimensional monocular and binocular eye movement records are shown.

I. Introduction

The instrument described in this article evolved from a series of experiments on the mechanisms of visual accommodation. Early in our accommodation studies, it became apparent that merely measuring the refractive power of the eye was not sufficient. We were also interested in isolating small retinal areas (to map sensitivity to blur over different regions of the retina) and in measuring the interaction between eye movements and the accommodation system. For these studies, the two measurement instruments described in this paper were developed to function simultaneously on the same eye: an optometer¹ to measure the refractive power of the eye and a double-Purkinje-image eyetracker² to measure the direction of the visual axis, both continuously. Experimental paradigms are much more restricted if accommodation measurements are limited to one eye, while eye-movement measurements are performed on the other eye.

This newly developed instrument system measures the point in three-dimensional (3-D) space on which the eye is fixated. The instrument can thus be thought of as a 3-D eyetracker. The direction of gaze is measured with a noise level and repeatability of about 1 min of arc rms. Refractive power is measured with a noise level of about 0.1 diopter.

The authors are with Stanford Research Institute, Menlo Park, California 94025.

Received 2 July 1977.

0003-6935/78/0301-0691\$0.50/0.

© 1978 Optical Society of America.

The fundamental operating principle of each instrument is discussed separately, followed by a description of the combined instrument.

II. Purkinje Eyetracker

Corneal and limbus eyetrackers can record very small eye movements, but their accuracy is poor. This inaccuracy arises from eye translation movements, which are indistinguishable from eye rotation movements. For example, 0.1 mm of eye translation causes approximately a 1° artifactual signal in the eye-rotation record from a corneal-reflection or limbus eyetracker.

The double-Purkinje method of eyetracking eliminates the translation artifact from the eye-rotation measurement. It is based on the use of a pair of reflections from optical surfaces of the eye. These reflections move by the same amount with eye translation but differentially with eye rotation. By monitoring the spatial separation of these two images, eye rotation can be measured accurately without being confused by translation. Similarly, eye translation can be measured accurately without being confused by eye rotation.

A. Purkinje Images

The virtual image formed by light reflected from the anterior surface of the cornea is known as the first Purkinje image, or corneal reflex [see Fig. 1(a)]. A second Purkinje image, formed by the component of light reflected from the posterior surface of the cornea, is almost coincident with the first Purkinje image. The light that is not reflected from either of these surfaces passes through the cornea, through the aqueous humor, and then through the lens of the eye. The third Purkinje image, a virtual image formed by the component of the light reflected from the anterior surface of the

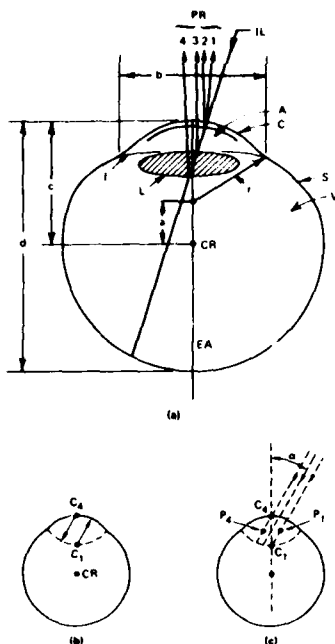


Fig. 1. (a) Schematic of the eye: *IL*, incoming light; *PR*, Purkinje reflections; *A*, aqueous; *C*, cornea; *S*, sclera; *V*, vitreous; *I*, iris; *L*, lens; *Cr*, center of rotation; *EA*, eye axis ($a \approx 6$ mm, $b \approx 12.5$ mm, $c \approx 13.5$ mm, $d \approx 24$ mm, $r \approx 7.8$ mm). The transmitted component of *IL* is refracted at each surface of the eye, as is each reflected component as it passes back through these surfaces. For simplicity, however, this refraction is ignored in the figure. (b) The first and fourth Purkinje mirrors essentially form a clamshell arrangement. C_1 and C_4 are the centers of curvature of the two respective mirrors. (c) Location of the first and fourth Purkinje images, P_1 and P_4 , for collimated input light at an angle α from the optic axis of the eye.

lens, is much larger and more diffuse than the other Purkinje images and is formed in a plane far removed from the plane of the other images. The fourth Purkinje image is formed by light reflected from the posterior surface of the lens at its interface with the vitreous humor. The rear surface of the lens acts as a concave mirror, forming a real image of the source.

The equivalent mirror surfaces that cause the first and fourth Purkinje reflection components form a basic clamshell arrangement. That is, the center of curvature for the first Purkinje mirror C_1 and the center of curvature for the equivalent fourth Purkinje mirror C_4 lie approximately within the opposite mirror surfaces [Fig. 1(b)]. Collimated light impinging on the eye at an angle α forms Purkinje images as shown in Fig. 1(c). The first Purkinje image, labeled P_1 , lies along the incoming ray passing through C_1 and at a distance equal to the focal length of the cornea (i.e., one-half of its radius of curvature). The fourth Purkinje image, labeled P_4 , lies along the ray passing through C_4 and at a distance equal to the focal length of the equivalent fourth Purkinje mirror (one-half of its radius of curvature). Because of the basic clamshell arrangement, both images lie almost exactly in the same plane, namely the pupil plane of the eye.

Although the fourth Purkinje image is almost the same size and is formed in almost the same plane as is the first Purkinje image, it is very dim because the difference in the refractive index between the lens and the vitreous humor is very small; the intensity of the fourth Purkinje image is less than $1/2\%$ that of the first Purkinje image.

A more detailed discussion of Purkinje image formation and movement is given in Ref. 2.

B. First-Generation Eyetracker

An early double-Purkinje-image eyetracker system is shown in Fig. 2. A light source *S* is imaged by lens L_1 onto stop S_1 , which defines the effective size of the light source. Stop S_1 is in the focal plane of lens L_2 . Therefore, an image of S_1 is formed in the focal plane of lens L_3 , which is made coincident with the pupil plane of the eye.

First and fourth Purkinje images are formed of stop S_2 , which is located in the focal plane of lens L_3 . Stop S_2 , therefore, appears to the eye at optical infinity. All the light emerging from stop S_2 passes through the image of S_1 formed at the eye.

First and fourth Purkinje images of stop S_2 are formed approximately in the plane of the eye pupil. Light from these images is, in turn, reflected by dichroic mirror *DC*, reimaged by lens L_4 , reflected by mirror *M*, and divided by beam splitter *BS*, to form two pairs of images. A_4 is a diaphragm containing a small round hole positioned to pass the fourth image to quadrant photocell P_4 . This diaphragm, which is attached to P_4 , blocks the light from the first Purkinje image. Beam splitter *BS* reflects about 10% of the incident light

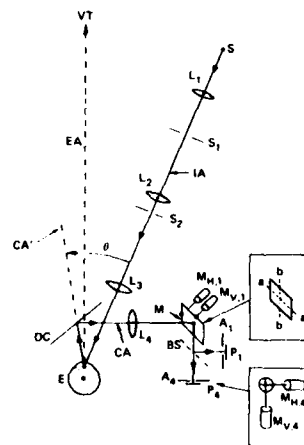


Fig. 2. Schematic of the first-generation eyetracker optical system: *E*, eye; *VT*, visual target; *IA*, input axis; *CA*, collecting axis; *CA'*, extension of collecting axis; *S*, light source; S_1 , stop imaged at pupil of eye; S_2 , source of Purkinje pattern, imaged at infinity; *DC*, dichroic mirror; *M*, front surface mirror; $M_{H,1}$ and $M_{V,1}$, motors that drive *M* in horizontal (yaw) and vertical (pitch) directions, respectively; $M_{H,4}$ and $M_{V,4}$, motors that drive P_4 in horizontal and vertical directions, respectively; *BS*, beam splitter; P_1 and P_4 , quadrant photocells; A_1 and A_4 , apertures in front of P_1 and P_4 , respectively.

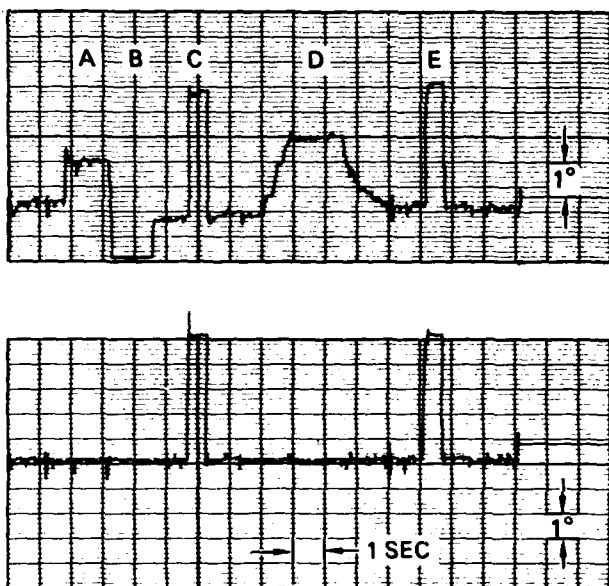


Fig. 3. Upper: horizontal eye movements recorded from first Purkinje image tracker while the subject fixates a target at infinity. Lower: simultaneous record from the fourth Purkinje image output. The upper track shows the wandering baseline, typical of corneal image trackers. During periods A and B, the subject leaned first one way and then the other way in the biteboard. During period D, the biteboard was translated laterally by ≈ 0.3 mm and then returned to its original position. Note the stability of the lower record during each of these intervals. During intervals C and E, the subject made voluntary eye movements of 5° .

toward another quadrant photocell P_1 , which detects the first Purkinje image. Diaphragm A_1 is positioned to block all light except that from the first Purkinje image.

Mirror M is pivoted at its center and is driven in yaw (around axis bb ; see inset) and pitch (around axis aa) by motors $M_{H,1}$ and $M_{V,1}$, respectively, which move to maintain the first Purkinje image centered on photocell P_1 . Control signals that drive these two motors are derived from signals from the four sectors of P_1 , which are arranged so that P_1 functions simultaneously as a horizontally oriented split-field cell and as a vertically oriented split-field cell.

Photocell P_4 is translated horizontally and vertically by motors $M_{H,4}$ and $M_{V,4}$, which move to keep the fourth Purkinje image centered on P_4 (see inset). Control signals that drive $M_{H,4}$ and $M_{V,4}$ are derived from the four quadrants of P_4 , which also operates simultaneously as a horizontally and vertically oriented split-field cell.

Mirror M thus maintains the first Purkinje image stationary on photocell P_1 , which is spatially fixed, while photocell P_4 is servocontrolled to track movement of the fourth Purkinje image relative to the first Purkinje image.³

If the eye translates, mirror M is automatically repositioned to maintain the first Purkinje image centered on P_1 ; the same movement properly repositions the

fourth Purkinje image as well, and no movement of P_4 results. If the eye rotates, however, the images move differentially, and the position of P_4 changes accordingly. The position of P_4 thus indicates the separation between the first and fourth Purkinje images and is a measure of the two-dimensional (2-D) angular position of the eye.

The signals that drive the servos are generally referred to as error signals; the servos move until the error signals become zero. The error signals could themselves provide a direct measure of image movement without the servos, but in that form of system (generally referred to as open loop) the magnitudes and the linearity of the output signals are very sensitive to factors such as component drift and change in gain in both the photodetectors and amplifiers, variation in light sensitivity across the face of the photodetectors, and the uniformity, shape, and brightness of the light pattern. The servos, by maintaining each image fixed at an electrical null position on its respective photocell, eliminate the sensitivity to these parameters and result in a much more stable system.

Figure 2 is actually a schematic of the first-generation eyetracker described in Ref. 2.

C. Demonstration of Translation Insensitivity

Figure 3 shows the horizontal motion of the eye while fixating a target. The top record is the horizontal motion of the 2-D mirror driven from the first-Purkinje-image cell. The bottom record is the horizontal movement of the fourth-Purkinje-image photocell [or the movement of the mirror driven by the stationary fourth Purkinje photocell in the new system (see Fig. 4)]. The first Purkinje record has a wandering baseline, typical of corneal (or limbus) eyetrackers, that results from translation-induced errors, whereas the signal from the fourth cell is independent of translation effects.

For the record of Fig. 3, a tight fitting dental plate (biteboard) was used. During period A, the subject was asked to lean to the left in the biteboard, and during period B to lean to the right. Note that whereas the lower record is immune to such movement, the upper record shows an output variation of almost $\pm 2^\circ$, indicating a movement of the head with respect to the biteboard of approximately ± 0.2 mm. During period D, the subject's head was translated approximately 0.3 mm to the left (with respect to the instrument) and then returned to its original position. Note the 3° output variation in the upper record and again the stability of the lower record (taken from the fourth Purkinje image output). During periods C and E, the subject made voluntary eye movements of 5° amplitude indicating the ability of both systems to record actual rotation movements of the eye.

Figure 3 indicates the difference between sensitivity and accuracy. A corneal, or limbus, tracker can detect very small eye movements, but its accuracy, or repeatability, is limited by the artifactual effects produced by translation movements of the eye. We have recorded drifts of 1 – 2° that are indistinguishable from rotation

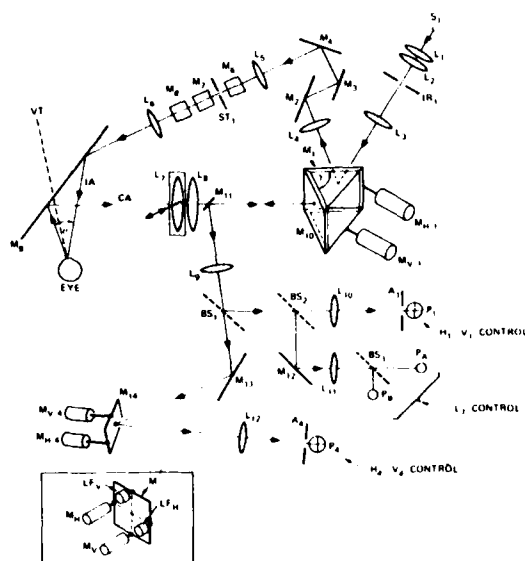


Fig. 4. Schematic of new eyetracker system: S_1 , IRLED source; IR_1 , adjustable iris conjugate with eye pupil; M_1 and M_{10} , coupled front-surface mirrors under control of motors $M_{H,1}$ and $M_{V,1}$; γ , angle between mirrors M_1 and M_{10} ; $M_2, M_3, M_4, M_6, M_7, M_8, M_{11}, M_{12}$, and M_{13} , front surface mirrors (mirrors M_2, M_3, M_4 , and M_5 , not shown, are used in different combinations to alter the angle θ of the incoming illumination); M_{14} , front-surface mirror driven by motors $M_{V,4}$ and $M_{H,4}$; M_9 , dichroic mirror; BS_1 , 90/10 pellicle beam splitter; BS_2 and BS_3 , 50/50 beam splitters; P_1 and P_4 , quadrant photocells; A_1 and A_4 , apertures in front of P_1 and P_4 , respectively; P_A and P_B , photocells in automatic focus-detection circuit; VT , visual target; IA , input axis; CA , collecting axis; stop ST_1 , source of Purkinje image pattern; LFH and LFV , linear followers.

of $1-2^\circ$ during a recording span of less than 1 min even with the head held rigidly by a tight-fitting dental-impression plate with the extra support of a forehead rest. In this case, translation-induced effects must be attributable in large part to movements of the eye within its socket.

III. Second-Generation Eyetracker

The new double-Purkinje-image eyetracking system is shown in Fig. 4. This version, which combines many substantial improvements over the first-generation instrument, greatly extends its performance and is easier to use.

A. Input Optics

S_1 is a solid-state light source with a narrow spectral band centered at $0.93\text{-}\mu\text{m}$ wavelength. Light from S_1 is electronically chopped at high frequency (4 kHz) to avoid the effects of room light and to use ac-coupled amplifiers in the Purkinje image servosystems thereby improving stability and decreasing noise.

Lenses L_1 and L_2 image S_1 into the plane of an iris diaphragm IR_1 , which is conjugate with the pupil of the subject's eye. Lens L_3 is positioned one focal length from the iris so the light emerging from L_3 is collimated.

This light is reflected from servoed mirror M_1 and imaged by lens L_4 . Assume for the moment, however, that mirror M_1 is fixed.

Lens L_5 is positioned one focal length from the image of the light source formed by lens L_4 . The required pathlength ($f_4 + f_5$) between lenses L_4 and L_5 is obtained by the multiple reflections provided by mirrors M_2, M_3 , and M_4 . An odd number of reflections from these mirrors provides an inversion of the horizontal component of the input light path. This inversion is necessary for the proper functioning of mirror M_1 , by means of which, as described later, the input light is made to track automatically any change in eye position.

Mirrors M_6, M_7 , and M_8 form a Dove mirror system to provide an inversion of the vertical component of the illumination system, which is also necessary for proper input-light tracking. Within the Dove mirror system is a stop ST_1 , a circular aperture approximately 2.54 cm (1 in.) in diameter. This aperture determines the size and shape of the Purkinje images formed at the eye and is in the focal plane of lens L_6 . Thus, light emerging from lens L_6 is collimated with respect to the image of the aperture. The eye is in the focal plane of lens L_6 and is illuminated by the light coming from the light emitting diode. Dichroic mirror M_9 reflects both the illumination light and the light reflected from the first and fourth Purkinje images that form in the subject's eye.

B. Output Optics

The Purkinje images are formed in the pupil plane of the eye, which is in the focal plane of output lens L_7 . Thus, light from the Purkinje images is collimated between lenses L_7 and L_8 . The light that passes through lens L_8 is reflected from mirror M_{10} onto mirror M_{11} , which is in the focal plane of lens L_8 .⁴ Because lenses L_7 and L_8 have the same focal length, a unity magnification image of the pupil plane of the eye is formed at mirror M_{11} .

Mirror M_{11} is in the focal plane of lens L_9 . Therefore, the light emerging from lens L_9 is collimated. Beam splitter BS_1 reflects approximately 10% of the incident light toward beam splitter BS_2 . The remaining light passes through BS_1 to front-surface mirror M_{13} . Beam splitter BS_2 reflects and transmits approximately equal amounts of light. The transmitted light is imaged by lens L_{10} onto the four-quadrant detector P_1 , which is in the focal plane of L_{10} . P_1 is therefore in a plane conjugate to mirror M_{11} and the pupil plane of the eye; aperture A_1 defines the size of field seen by P_1 . Thus, when the first Purkinje image is at one particular point on mirror M_{11} (or in the pupil plane of the eye), it will fall on the center of the four-quadrant photodetector. If the image tends to move away from this point, the image at the detector will move, and the resulting error signals will drive servomotors $M_{H,1}$ and $M_{V,1}$ to reposition mirror M_{10} (and mirror M_1). The mirror is repositioned in yaw and pitch to bring the first Purkinje image to its initial point on mirror M_{11} and thus on the

photodetector. In this way, the image of the eye formed at mirror M_{11} always has its corneal reflection in the same location.

The light reflected from beam splitter BS_2 reflects from front-surface mirror M_{12} and is imaged by lens L_{11} (and split by a 50/50 beam splitter BS_3) onto two focus-detecting photodiodes P_A and P_B . These photodiodes are displaced axially approximately 0.5 cm on either side of the plane of focus of the first Purkinje image and, being small in size, measure light-flux density along the axis of the imaging system. When the eye is in the correct position axially, each of these photodiodes receives the same amount of light. If the eye moves axially, one or the other of these photodiodes receives more light, and the difference in light level generates an error signal for a servomotor that drives the carriage containing lens L_7 . As described later, lens L_7 is repositioned so the two photodetectors continually receive equal amounts of light. This ensures that the first Purkinje image is always in focus on P_1 in spite of axial eye movement.

The light transmitted by beam splitter BS_1 reflects from mirror M_{13} onto the servoed mirror M_{14} and is collected by lens L_{12} . At the focal plane of lens L_{12} is a second four-quadrant photodetector P_4 , which receives the fourth Purkinje image; aperture A_4 defines the size of field seen by P_4 . Signals derived from quadrant cell P_4 control motors $M_{H,4}$ and $M_{V,4}$. These motors move mirror M_{14} in yaw and pitch to keep the fourth Purkinje image centered on P_4 .⁵

Opposite each mirror motor is mounted a linear motion follower LF with a sensitivity better than $1\ \mu\text{m}$ (see inset of Fig. 4). These motion sensors are used in a local internal servo feedback loop in each driver circuit to achieve high frequency response and to minimize hysteresis and dead zone. Signals from $LF_{H,1}$ are used in the servo loop that drives motor $M_{H,1}$, and signals from $LF_{V,1}$ are used in the servo loop that drives motor $M_{V,1}$. Similar motion sensors are used in conjunction with drive motors $M_{H,4}$ and $M_{V,4}$.

The direction of the eye axis, i.e., the angle of gaze, is derived directly from $LF_{H,4}$ and $LF_{V,4}$ signals, as described earlier. Signals from $LF_{H,1}$ and $LF_{V,1}$ represent the horizontal and vertical positions of the first Purkinje image, which moves in response both to eye translation and eye rotation. By properly combining the signals from $LF_{H,4}$ and $LF_{V,4}$ with those from $LF_{H,1}$ and $LF_{V,1}$, one can also accurately track the translational position of the eye.

C. Automatic Input-Path Tracking

The new instrument is designed to permit up to a centimeter of eye position variation in all dimensions: horizontal; vertical; and axial. For a large axial variation to be tolerated, it is necessary to incorporate automatic focus into the eyetracker (see the next section on automatic focus). For large lateral variations to be tolerated, either a large input beam must be used, so the eye never moves out of the beam, or the input light path must track eye position automatically, in which case a

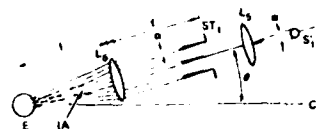


Fig. 5. Translation of the source S_1 , or source image S_1' , moves the image at the eye but does not change the angular separation θ between the input axis IA and collecting axis CA . A cone of size α will emerge from each point of the pattern in stop ST_1 , where α is the angular size of the source image S_1' as seen from lens L_6 .

small light source can be used. The latter option was chosen because it offers many advantages: less total light energy directed toward the eye; a crisper fourth Purkinje image because of less stray light; and improved automatic capture because the first Purkinje tracker can sometimes lock onto the iris if it is illuminated.

For automatic input-path tracking, mirror M_1 (in the input path of Fig. 4), which was assumed fixed in the earlier discussion, is used to keep the illumination beam centered on the pupil. For this purpose, mirror M_1 is rigidly connected to, and therefore moves in synchronism with, mirror M_{10} .

To understand how the input light is made to track eye position, note that, if the eye moves upward, the corneal reflection tends to move upward on detector P_1 . Error signals generated by this photodetector reposition mirror M_{10} to maintain the corneal image centered on M_{11} . Motion imparted to M_{10} , however, also repositions mirror M_1 ; this automatically deflects the illumination beam upward to track the corneal reflection. However, the illumination tracking cannot be perfect with respect to the pupil of the eye because P_1 tracks the corneal reflection, which moves with respect to the eye pupil when the eye makes rotational movements. Nevertheless, the design is such that the tracking error is less than 1 mm with eye translation of ± 0.5 cm in any direction and with eye rotations of 15° in all directions (30° diam field), that is, the input illumination beam tracks the center of the pupil to within 1 mm over this range.

A critical requirement of the input-light tracking system is that a shift in the input light path must not cause any change in the angle of the input axis IA with respect to the eye axis. Any such change would alter the separation of the Purkinje images and therefore be interpreted as an eye rotation. This situation is avoided as follows.

Figure 5 shows the light entering the eye directly at an angle θ to the collecting axis. (For simplicity, the dichroic mirror is not shown.) The input system consists essentially of lens L_6 located at its focal length from the eye and stop ST_1 located one focal length away from L_6 . Stop ST_1 therefore appears to the eye to be at infinity. Stop ST_1 is illuminated by S_1' , which is an image of iris IR_1 and is in the focal plane of lens L_5 . The light cones emerging from each point of ST_1 are collimated by lens L_6 , and their intersection at the eye is an image of S_1' and therefore of iris IR_1 .

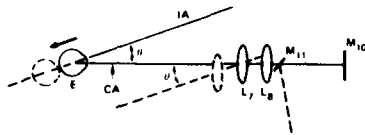


Fig. 6. Focus adjustment by translating lens L_7 along a path parallel to the input axis IA . This method of focus adjustment maintains constant optical magnification over the focus range and maintains a constant final image position when the eye translates along the input axis. CA , collecting axis; θ , angle between CA and IA .

If iris IR_1 were translated in its own plane, its image S_1' , and hence the image of S_1' at the eye, would similarly translate, but the collimated ray bundles from each point of ST_1 would not change their angular orientation, as desired. It is therefore possible to achieve the desired input tracking simply by translating the iris. However, that would require yet another 2-D servosystem. Instead, the same effect is achieved by placing mirror M_1 in the collimated light path between lenses L_3 and L_4 (in Fig. 4) and attaching it rigidly to mirror M_{10} , as described above. The required movement sensitivity in the input light path is obtained by the proper choice of angle γ (see Fig. 4) between mirrors M_1 and M_{10} .

D. Automatic Focus

To obtain the desired 1 cm of allowed axial variation in eye position, an automatic focus system tracks the axial position of the eye. Without automatic focus, intolerable blurring of the Purkinje images would occur at the quadrant photocells.

The automatic focus system must meet two stringent requirements: First, any change in focus must not cause any change in optical magnification. A change in magnification would result in a change in separation of the two Purkinje images and, therefore, be interpreted as an eye rotation. Figure 6 shows the eye and the two output lenses L_7 and L_8 ; again, for simplicity, the dichroic mirror is not shown. The Purkinje images are in the focal plane of lens L_7 . Because the light between lenses L_7 and L_8 is collimated, the eye and lens L_7 can both move along axis CA without any change in magnification in the final image, as long as the distance between the eye and lens L_7 remains constant. The first step in automatic focus, therefore, is to have the axial position of lens L_7 track the axial position of the eye.

The second requirement is that the input light not shift if the eye translates along the input-light axis IA . In that case, the input light is already aimed directly at the eye, and any shift would move the light away from the eye. In other words, the automatic focus system must be designed so eye translation along the input axis does not cause any shift in mirror M_{10} , which in turn requires that there be no change in the position of the first Purkinje image. This is achieved by shifting lens L_7 not along axis CA , but along the path parallel to the input-light path IA , as shown by the dashed line of Fig. 6. Again, because the light between lenses L_7 and L_8 is collimated, an equal lateral component of shift of the

eye and lens L_7 will not change the position of the final image formed by lens L_8 . A shift in eye position along any other axis will, however, shift the input-light path appropriately as well as activate the automatic focus system.

In Fig. 4 we noted that the signal that drives the focus servosystem derives from the difference in signals from photocells P_A and P_B . This signal is zero when the first Purkinje image is in focus on quadrant photocell P_1 .

Output from the servosystem that drives L_7 provides a direct measure of the axial position of the eye. Combined with the horizontal and vertical eye position signals described earlier, the 3-D position of the globe can thus also be accurately tracked separately from the angular orientation of the globe.

E. Automatic Search

An automatic search of the field is made whenever the first Purkinje system becomes unlocked, as indicated by an improper light level falling on photocell P_1 . In this case, the first Purkinje mirror is made to sweep in an increasing spiral from the central position, and the focus servosystem returns to its central position. On the average, recapture occurs about $1/2$ sec after the initiation of a search action. When successful capture has been achieved by the first Purkinje system, the focus servosystem is reactivated, and a small-field spiral search is initiated by the fourth Purkinje system. (With the first Purkinje system locked, the fourth Purkinje image falls within a small, well-defined area.) Again, the average capture occurs about $1/2$ sec after initiation of a search action, for a total average search-and-capture of about 1 sec. Separate light-level detectors in the fourth Purkinje system indicate when the fourth system is operating normally. A search for the fourth image is automatically initiated whenever the fourth light level is out of range.

A separate output signal indicates whenever the first or fourth Purkinje tracker is unlocked for any reason. The signal can be used to ignore those portions of the eye records in manual or automatic processing of the data.

IV. Optometer Principles

A. General

Reference 1 describes the basic form of the optometer that is combined with the double-Purkinje-image eyetracker in the 3-D instrument. In this section, we discuss the basic principles of the optometer.

Figure 7 is an optical diagram of the eye viewing a point source through a small aperture. In Fig. 7(a), the refractive power of the cornea and lens are such that the point is sharply imaged on the retina. In this case, if an aperture were moved from position A to position B , different bundles of rays from the source would strike the retina, but the illuminated retinal spot would be stationary. In Fig. 7(b), the refractive power of the eye is too small, and the retinal spot moves from position A' to B' in response to aperture movement from A to B .

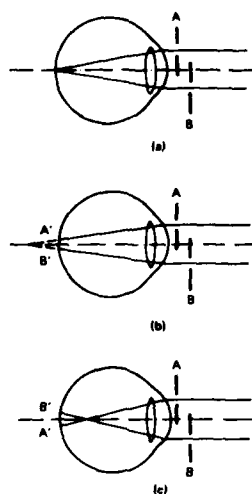


Fig. 7. Imaging a point target at infinity through a small aperture that alternates between two positions, *A* and *B*. The intercepted-ray position at the retina will be stationary or will move with or move opposite to the aperture, respectively, according to whether the eye is focused for infinity (a), beyond infinity (b), or closer than infinity (c).

Conversely, in Fig. 7(c), the refractive power of the eye is too great, and the retinal spot moves from *A'* to *B'* (i.e., in the opposite direction) in response to aperture movement from *A* to *B*. The object plane conjugate to the retina can be found by changing the distance of the source, according to the polarity of the image movement, until the retinal image is stationary. The optometer performs this function automatically and continuously.

Figure 8 illustrates the basic optometer configuration. Instead of a mechanical aperture positioned close to the eye, an optical projection system achieves the same effect. Two adjacent, near-ir light sources, *S*₂ and *S*₃, which have a narrow spectral band centered at 0.93- μ m wavelength, are located in the focal plane of lens *L*₁.⁶ An image of the light sources is formed in the plane of the pupil of the eye, which is at the focal plane of lens *L*₂. The light sources flicker on and off alternately at a rate of 400 Hz. Thus, light enters the eye first through one small area of pupil (the image of the first light source) and then through an adjacent area of the pupil (the image of the second source). This is equivalent to two alternating aperture positions.

Stop *ST*₂, which is illuminated alternately by sources *S*₂ and *S*₃, appears to the eye at a virtual distance

$$L = (f_2)/(1 - [d/(f_2)]), \quad (1)$$

where *L*, *d*, and *f*₂ (the focal length of lens *L*₂) are in meters. To focus stop *ST*₂ on the retina requires an accommodation level

$$D_E = \frac{1}{L} = \frac{1}{f_2} \left(1 - \frac{d}{f_2}\right), \quad (2)$$

where *D*_E is in diopters. We use the convention that the refractive power of the eye is stated relative to its power when accommodated for infinity (i.e., when *d* =

*f*₂, *D*_E = 0 diopters). As the eye changes its refractive power, stop *ST*₂ is maintained in focus on the retina by adjusting *d*, whose position is a direct measure of the instantaneous refractive power of the eye. Note from Eq. (2) that *D*_E, measured in diopters, is linearly related to the distance *d* measured in meters.

Stop *ST*₂ is moved along the optical axis in response to the movement of the image of stop *ST*₂ on the retina. This movement is detected by reimagining the retinal image onto a split-field photocell *SFP* and sensing lateral movement of the image in synchronism with the alternation of light sources *S*₂ and *S*₃. If stop *ST*₂ is in focus on the retina, the image will be stationary. If the image is out of focus, it will appear to move either in phase or out of phase with the alternation of the light source, as illustrated in Fig. 7.

The image formed at the photocell derives from light reflected from the retina, which passes back out through the pupil of the eye. This light is reflected by dichroic mirror *M* and then by beam splitter *BS*. If *ST*₂ is in focus on the retina, lens *L*₃, which is identical to lens *L*₂, forms an image of the retinal image in a plane that is conjugate with stop *ST*₂ (i.e., at plane *RI*, which is at a distance *d* from lens *L*₃). For clarity, lens *L*₃ is drawn adjacent to lens *L*₂, as though the dashed portion *W* of the output path were of zero length; actually, *L*₃ is located at the same optical distance from the eye as is *L*₂. Split field photocell *SFP* could be located in plane *RI* except that it is necessary first to block the corneal reflection, which is much brighter than the reflected retinal image. Thus, the image in plane *RI* is relayed by a pair of fixed lenses *L*₄ and *L*₅. With *L*₄ and *L*₅ separated by a distance equal to twice their focal length, the retinal image formed in plane *RI* is relayed a distance equal to four focal lengths (see next section), as shown in Fig. 8, in which plane *SFP* is located. An image of the plane of the pupil is obtained in the focal plane of lens *L*₄, which is conjugate also to the plane of the light sources *S*₂ and *S*₃. A small corneal stop (*CS*) placed in this plane blocks the very small but bright corneal reflection of sources *S*₂ and *S*₃.

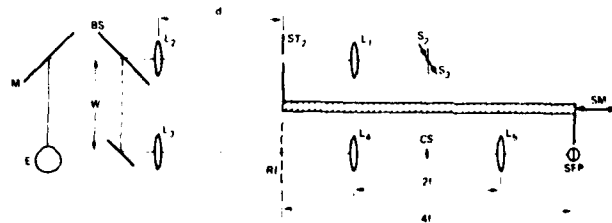


Fig. 8. Basic optometer arrangement: *S*₂ and *S*₃, IRLEDs; *ST*₂, stop that is imaged on the retina; *M*, dichroic mirror; *BS*, beam splitter; *CS*, corneal stop; *SFP*, split-field photocell. *ST*₂ and *SFP* are linked mechanically to slide *SM*. The number of diopters of accommodation required by the eye to focus on *ST*₂ is linearly related to the distance *d* between *ST*₂ and *L*₂. When *ST*₂ is in focus on the retina, the retinal image is also reimaged at plane *RI*, which is relayed by fixed lenses *L*₄ and *L*₅ to the plane of *SFP*. For simplicity, *L*₃ is drawn opposite *L*₂, although the entire output path should be shifted to the left by the distance *W*.

Stop ST_2 and the SFP are mechanically linked. Thus, when stop ST_2 is in focus on the retina, the retinal image will be conjugate with, and therefore stationary on, the split-field cell. If ST_2 is out of focus, movement of the image on the retina in one phase or the other will drive the slide SM in the appropriate direction until the error signal is zero, and the image is stationary on the retina and therefore on the photocell. If the servosystem has a faster response than the accommodation system of the eye, the instantaneous position of the slide (i.e., distance d) will provide an accurate measure of the instantaneous refractive power of the eye.

B. Optometer Range

From Eq. (2), we see that $D_E = 1/f_2$, when $d = 0$. Thus, the maximum measurable diopters is equal to the focal length (in diopters) of lens L_2 . To measure an accommodation level up to +20 diopters, for instance, lens L_2 would require a focal length of 1/20th m, or 50 mm. The problem with such a short focal length lens is that it must be brought very close to the eye, and there is very little room for other optical elements that might be needed.

A way to increase this distance and the diopter range at the same time is to use an image of stop ST_2 instead of the stop itself. The problem with a real stop, of course, is that it cannot pass through the lens. That is, we cannot achieve negative values of the distance parameter d . But an image can pass through the lens, and in that way the power of the instrument can be increased beyond the power of lens L_2 . [Equation (2) holds exactly even for negative values of d .] This fact is important in combining the eyetracker and optometer, which is discussed in the next section.

V. Combined Three-Dimensional Instrument

The major task in building a composite instrument was to combine an optometer instrument of the form shown in Fig. 8 with the eyetracker shown in Fig. 4. To help the reader appreciate how the merging was achieved, we must discuss briefly a certain basic feature of a telescope.

The simplest telescope consists of a pair of positive lenses separated by a distance equal to the sum of their focal lengths. Although telescopic systems have undergone extensive study and many practical developments, here we are concerned only with certain properties and uses of the telescope as a relay system.

With a pair of lenses separated by the sum of their focal lengths, it is easy to show that the object and image distances, p and q , measured from each lens, as shown in Fig. 9, have the following linear relationship:

$$q = f_2 \left(1 + \frac{f_2}{f_1} \right) - \left(\frac{f_2}{f_1} \right)^2 p. \quad (3)$$

where f_1 and f_2 are the focal lengths of the two lenses. As a result, both the axial magnification ($\Delta q / \Delta p$) and the lateral magnification ($M = f_2 / f_1$) are constant, independent of distance p . Although apparently not well known, it is therefore possible with this configuration (for the case $f_2 = f_1$) to achieve imaging with neither

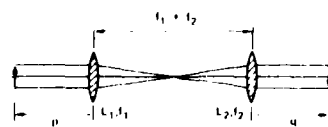


Fig. 9. Telescope configuration. With two lenses separated by the sum of their focal lengths, the object and image distances, p and q , are linearly related, and lateral magnification is independent of p .

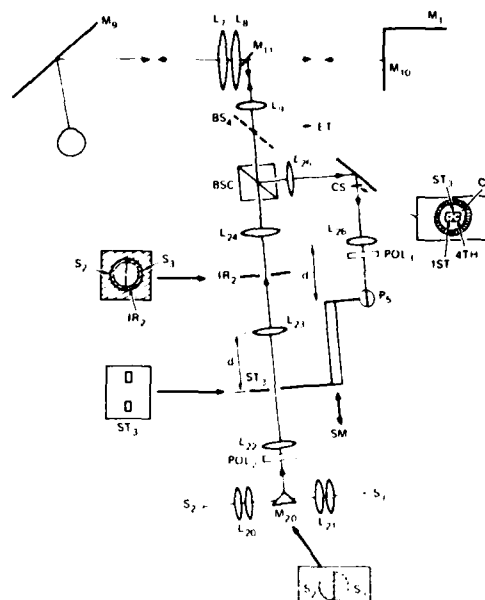


Fig. 10. Merging the two instruments. The instruments are merged by means of beam splitter BS_4 . ET , remainder of the eyetracker system; BSC , polarizing beam splitter cube; S_2 and S_3 , IRLEDs; M_{20} , 90° mirror that merges the images of S_2 and S_3 ; ST_3 , stop that is imaged on the retina; IR_2 , adjustable iris conjugate with the eye pupil plane; P_5 , split-field photocell on which the retinal image falls; CS , corneal stop; POL_2 and POL_3 , polarizers that reinforce the input and output polarization directions of BSC ; ST_3 and P_5 are linked mechanically to slide SM .

axial nor lateral distortion (at least to a first-order approximation); compare this case with single-lens imaging, in which axial and lateral magnification both vary with the object-to-lens distance (see Fig. 3 of the accompanying paper⁷).

Of specific interest to this discussion is that the object and image distances are linearly related, even for $f_2 \neq f_1$. In fact, just as Eq. (2) is true for an object on the far side of the lens (negative values of d), so too it is readily shown that Eq. (3) is true for an object (or an image of an object) that falls between the two lenses of Fig. 9 and even beyond the right-hand lens (i.e., negative values of p). Thus, a telescopic relay in the optometer path does not alter the linear relation between eye diopters and the movement of stop ST_2 .

In Fig. 4, lenses L_7 and L_8 together form a unity magnification image of the Purkinje reflections at mirror M_{11} , which is the focal plane of lens L_9 . Looked at another way, lens L_7 is a focal distance from the pupil

plane of the eye and plays the role of lens L_2 in Fig. 8, while lenses L_8 and L_9 , which are separated by the sum of their focal lengths, together form a (nonunity ratio) telescope system. By merging the optometer with the eyetracker on the distal side of lens L_9 as viewed from the eye, we benefit from the first-Purkinje-image stabilization provided by mirror M_{10} , while maintaining the linear relation of Eq. (2) between eye diopters and servo motion. We can also obtain a large diopter range even though lens L_7 is of relatively long focal length; see Sec. IV.B. The main disadvantage of this scheme is that lenses L_7 , L_8 , and L_9 are now common to the input and output paths of the optometer. Any reflection of optometer input light from these lens surfaces that enters the optometer output path can cause serious artifact signals because the total light reflected from the fundus of the eye is extremely small. Elimination of these reflections requires special care.

A schematic of the composite instrument is shown in Fig. 10. The two instruments are merged via beam splitter BS_4 , which is mounted between lens L_9 and beam splitter BS_1 (see Fig. 4). Although BS_4 reflects the optometer light at right angles to the plane of the paper of Fig. 4, BS_4 is shown as transmitting, rather than reflecting, so the optometer and relevant eyetracker optics can be drawn in a single plane.

A. Optometer Input Path

Light sources S_2 and S_3 are imaged by lens pairs L_{20} and L_{21} onto a right-angle mirror M_{20} , which causes two half-disks of light to appear side by side, as shown in the lower inset to Fig. 10. The two half-disks of light are energized out of phase. An image of this flickering light pattern, which is in the focal plane of lens L_{22} , is formed on iris diaphragm IR_2 located in the focal plane of lens L_{23} and also in the focal plane of lens L_{24} . (Lenses L_{23} and L_{24} , which are identical and are separated by twice their focal length, form a unity ratio relay lens.) Another image of the light sources S_2 and S_3 is thus formed on mirror M_{11} , which, as explained earlier, is conjugate to the pupil plane of the eye. The diameter of the light source pattern at the eye pupil plane is adjustable by means of iris IR_2 (see inset, Fig. 10).

Stop ST_3 and lens L_7 together are functionally equivalent to stop ST_2 and lens L_2 in Fig. 8, except that they are separated by two relay lens pairs, (L_8 , L_9) and (L_{23} , L_{24}), in series. (Relay lens pairs in series have the same linearity properties as a single lens pair.) With stop ST_3 positioned so that its image is in the focal plane of L_9 , light from ST_3 reaching lens pair L_7 and L_8 is collimated, and another image of ST_3 is formed halfway between L_7 and the eye, a distance $f_7/2$ from the eye (which represents nine diopters of refractive power). As ST_3 moves farther from (or closer to) L_{23} , the final image moves farther from (or closer to) the eye, i.e., to a position of less (or more) dioptric power.

Stop ST_3 is a narrow slit with its center blocked (see the inset on the left of Fig. 10). The reason for blocking the center is that very bright, on-axis, input light would

be reflected directly back by mirror M_{11} (after reflection from M_{11} to M_{10} and then back toward L_8) and could cause a serious artifact in the optometer output signal.

B. Optometer Output Path

Lenses L_{25} and L_{26} are conjugate with lenses L_{24} and L_{23} , respectively. A corneal stop CS is located in a plane conjugate with iris IR_2 . If stop ST_3 is in focus on the retina, an image of the retinal image is formed at a distance d from lens L_{26} . The split-field cell P_5 is placed in this plane, as shown in Fig. 10. If ST_3 is out of focus on the retina, its image on the retina moves in synchronism with S_2 and S_3 . This side-by-side motion is detected by P_5 , and the resulting signal drives the slide containing ST_3 until the retinal image is again stationary.

Potentially large artifact signals can be generated in the optometer output by specular reflections of optometer input light from lenses L_7 , L_8 , L_9 , and the cornea, which are common to the input and output paths of the optometer. This potentially serious artifact is eliminated by polarizing the optometer input light with a polarizing beam splitter cube BSC . Any specularly reflected light from lenses L_7 , L_8 , L_9 , and the cornea has the same polarization as the input light and, therefore, will not be reflected into the optometer output path, but will pass directly back through the BSC .

Polarizers POL_2 and POL_3 , shown in the optometer input and output paths in Fig. 10, are not logically necessary, although they are important for proper functioning. Polarizer POL_2 blocks the input light that would normally be reflected by BSC , thus substantially reducing the magnitude of light that may be rereflected from the external surface of BSC and that could reenter the output path. Further, because BSC is not a perfect polarizer, a certain amount of light is also scattered at its diagonal interface. POL_3 significantly reduces the amount of scattered light that enters the output.

C. Optical Isolation between the Two Instruments

Eyetracker light is blocked from the optometer by enlarging the corneal stop CS in the optometer output path. The inset on the right of Fig. 10 shows the Purkinje reflection from the optometer, labeled ST_3 , and from the eyetracker, labeled 1st and 4th. The BSC prevents most of the optometer light that is reflected from the cornea from reentering the output path of the optometer. However, this reflected light is so bright that it is still necessary to use a corneal stop CS that is large enough to block the corneal image of ST_3 . By enlarging the stop, as shown in the inset in Fig. 10, light from the first and fourth images from the eyetracker is also blocked. The stabilizing action of the eyetracker keeps the corneal reflection blocked by the stop CS even under conditions of eye rotation and/or translation.

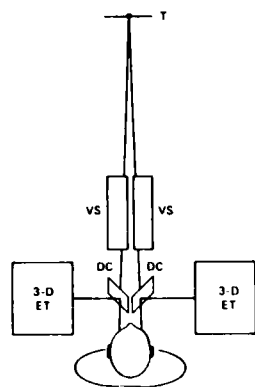


Fig. 11. Subject configuration for stimulating and recording 3-D eye movements: 3-D-ET, 3-D eyetracker, which includes dichroic mirror DC; VS, 3-D visual stimulator; T, target.

D. Electrical Isolation of the Instruments

Most of the eyetracker light is eliminated from the optometer by the enlarged corneal stop as noted above. In the eyetracker, the effects of a bright corneal image of the optometer input falling on top of a weak fourth Purkinje image (in certain directions of gaze) are eliminated by a high-pass electrical filter, which creates a single-sideband system for the 4-kHz eyetracker signal. This filter eliminates any 400-Hz signals from the eyetracker channels. A combination of low-pass and bandpass filters removes from the optometer signal any residual 4-kHz eyetracker signals.

VI. Performance

A. Binocular Configuration

Figure 11 shows a binocular configuration with which the records of this section were taken. Each eye views a target *T* through a dichroic mirror (mirror *M*₉ in Fig. 4) and a 3-D visual stimulator *VS*. By means of three servocontrolled mirror and lens systems, *VS* can move the visual field horizontally and vertically independently and can vary the optical distance of the target without changing its brightness or size.⁷ The *VS* also provides a location for an artificial pupil, if desired. Movements of each eye are monitored by a separate 3-D eyetracker. Two such stimulator and eyetracker instruments aligned side by side in a binocular configuration provide independent visual stimulation and recording from each eye. Figure 12 is a photograph of a pair of 3-D eyetrackers and visual stimulators arranged in such a binocular configuration.

The focus stimulator portion of *VS* can be used as a focus corrector for subjects who normally wear glasses. Although the eyetracker has been operated with subjects wearing glasses, it is not the preferred method of operation. The *VS* can adjust spherical power to suit the subject, and cylinder power can be corrected with standard ophthalmic cylinder lenses inserted near the artificial pupil plane.

B. Three-Dimensional Records

Single-eye recordings are adequate to illustrate the basic response of the instrument. In Fig. 13, the right eye was occluded, and the left eye *VS* caused a fixation target to be moved simultaneously in a sawtooth pattern vertically and in a sine-wave pattern horizontally both 8° peak to peak. At the same time, the focus stimulator



Fig. 12. The 3-D, binocular arrangement.

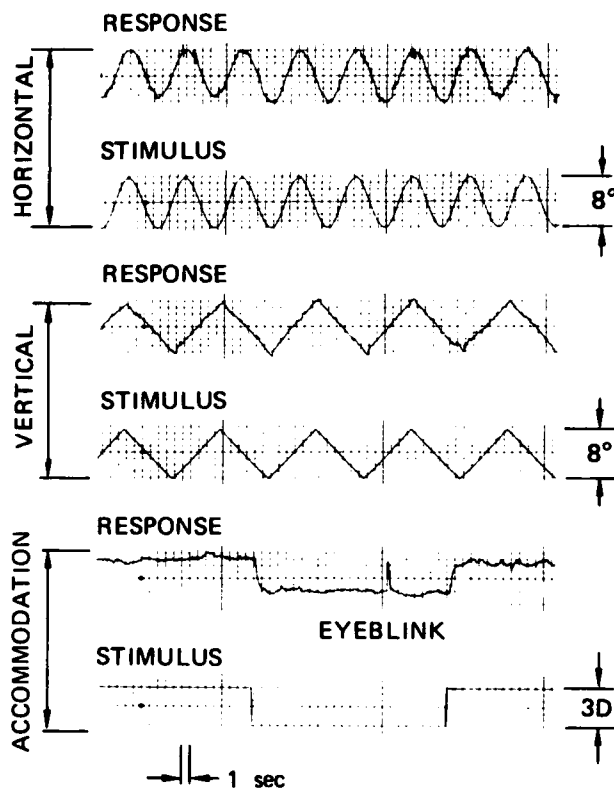


Fig. 13. 3-D, monocular recording made while the subject tracked a target moving horizontally according to an 8° sine wave, vertically according to an 8° sawtooth of different frequency, and in focus according to a 3-diopter square wave of still another frequency (right eye occluded).

altered the optical distance to the target between infinity (zero diopters) and a third of a meter (three diopters), according to a square-wave pattern. That is, the target movement in each dimension was independent of the form and frequency of the movement in the other dimensions.

C. Eyetracker and Optometer Response

The noise level in the X and Y channels of the 3-D eyetracker is less than 1 min of arc rms. The allowable range of eye movements varies from subject to subject, depending primarily on pupil size. A range of at least 20° is achieved easily with most subjects. The optometer has a range from -4 to $+12$ diopters and a noise level of approximately 0.1 diopter.

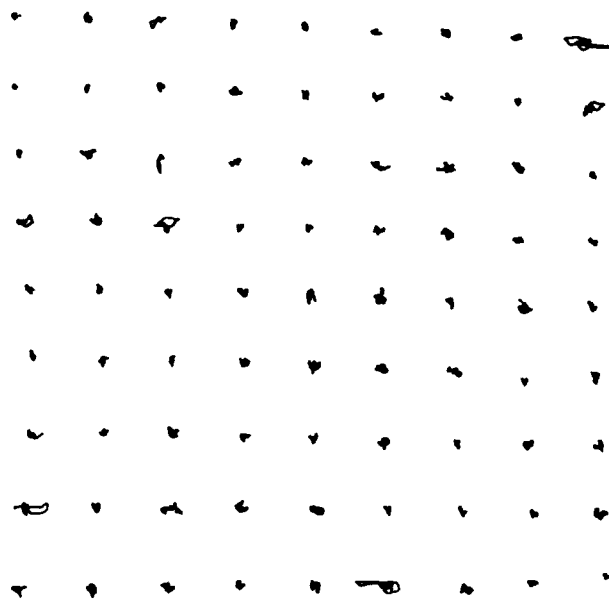


Fig. 14. Two-dimensional field plot; spacing between spots is 2° .

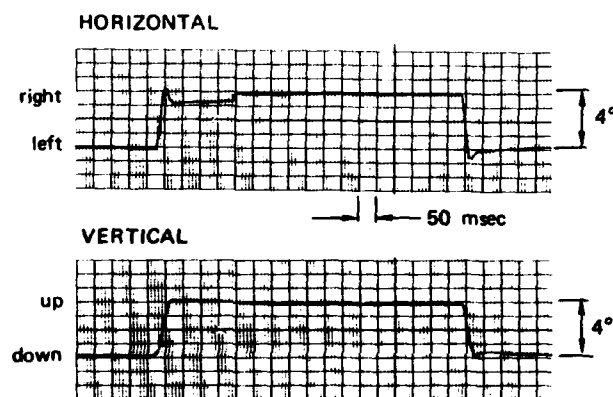


Fig. 15. Simultaneous horizontal and vertical eye movements, showing the general form of the response. Note the difference in horizontal and vertical eye movement velocities during the saccade.

Figure 14 is a 2-D field plot of the eyetracker made with an X-Y recorder. The X and Y inputs were driven directly from the horizontal and vertical outputs, H_4 and V_4 , of the fourth Purkinje tracker. For this plot, the subject moved his fixation voluntarily around a 9-by-9 matrix of bright points spaced 2° apart. The subject fixated on each point for several seconds; the pen was deenergized between fixation points.

Although there is a field distortion over large eye movements, repeatability is a few min of arc, that is, the plot retraces itself to that degree of accuracy even if the subject gets off the biteboard between plots.

The horizontal and vertical servos have a frequency response approximately flat to 300 Hz and a maximum slewing rate greater than $1000^\circ/\text{sec}$. Figure 15 shows the eye response to a diagonal step change having 4° horizontal and vertical components. Note that the horizontal velocity in the first saccade is almost twice that of the vertical velocity— $200^\circ/\text{sec}$ vs $100^\circ/\text{sec}$. The servos also have a lag of approximately 1 msec, which results in a 6-min of arc lag when tracking an eye movement of $100^\circ/\text{sec}$.

The dynamic response and the noise level of the eyetracker are adequate to achieve a stabilized-image disappearance of moderate contrast targets when the eyetracker signals are used to drive a CRT so that its pattern tracks the eye movements and thereby stabilizes the image on the retina.⁸ Good disappearance capability has also been demonstrated using the 3-D stimulator to stabilize a fixed visual pattern in space.

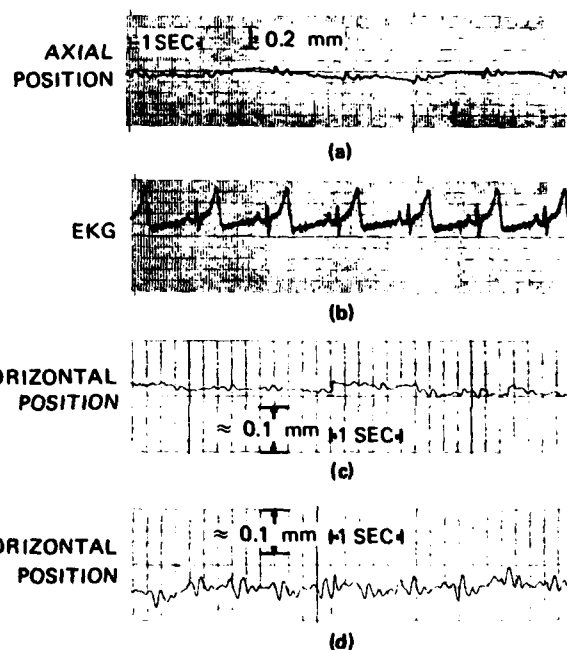


Fig. 16. Eye movement in response to heartbeat. These illustrate the sensitivity of the instrument in detecting 3-D translational as well as rotational motions of the globe. (a), (b) Axial eye motion and simultaneous EKG; horizontal eye motion (c) before and (d) after exercise.

D. Translation Sensitivity

The primary achievement of the Purkinje eyetracker is separation of the translation and rotation components of eye motion, as illustrated in the records of Fig. 3.

Although the eye rotation records are nominally independent of any translation motions of the eye, they are not completely independent over large translation motions. Moving the head laterally by ± 0.5 mm, which would cause an eye movement artifact of approximately $\pm 5^\circ$ with a corneal tracker, can result in an artifact signal of several min of arc. Translation sensitivity to axial motion can be of similar size—several min of arc/mm of axial movement of the eye. With the eye relaxed to infinity, the optometer output can change by approximately 0.1–0.2 diopter/mm of head movement in any direction. The source of this residual translation sensitivity has not been completely explored, so it is not clear how much further this residual interaction can be reduced.

The sensitivity of the instrument in detecting translation motions is illustrated in Fig. 16. Part (a) of Fig. 16 illustrates axial eye motions recorded from the focus-detector diodes P_A and P_B of Fig. 4, with the focus servo inactivated. A simultaneous EKG recording, Fig. 16(b), verifies that the repetitive pattern is that of the

heartbeat. Figure 16(c) shows a recording from the first Purkinje (horizontal) channel with the subject relaxed to infinity and voluntarily suppressing saccades. The heartbeat pattern does not show in the simultaneous fourth Purkinje record (not shown), indicating that the record is a pure translation motion of the eye (of approximately $30 \mu\text{m}$), or a rotation component that is too small to see in the fourth Purkinje record. After vigorous exercise, both the rate and the amplitude of these eye translation motions increase, as shown in Fig. 16(d).

E. Eyetracker Overshoots

The eyetracker output often shows brief overshoots at the end of saccades [see the lower trace of Fig. 17(a)]. The source of these overshoots appears to be relative lateral motion of the lens within the globe, inasmuch as similar motions do not appear at all or are much smaller in the output from the first Purkinje tracker (i.e., in the motion of the first Purkinje image) [see the upper trace of Fig. 17(a)]. If this is the correct explanation, we might expect the size of the overshoots to vary with accommodation level (i.e., with changes in the physical configuration of the suspension of the eye lens). That this is the case can be seen from Figs. 17(b) and 17(c)

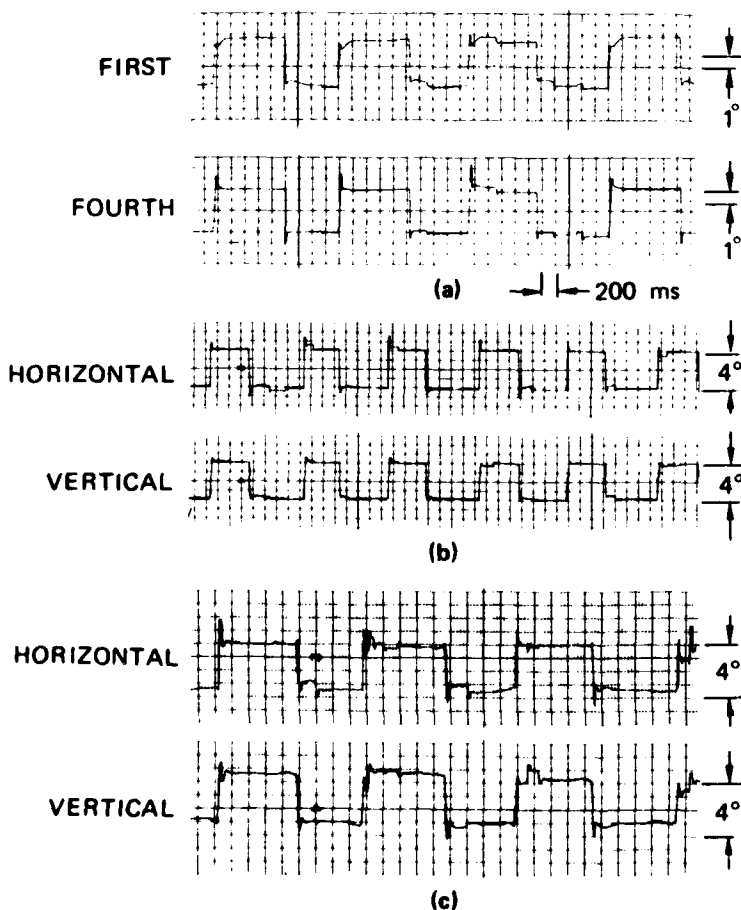


Fig. 17. Overshoots in the eye-movement records during saccades. As discussed in the text, these seem to be caused by lateral motions of the eye lens within the globe. (a) Simultaneous records from the first and fourth Purkinje image tracking systems. Note the small overshoots in the first Purkinje record and the large (and inconsistent) overshoots in the fourth Purkinje record. The 100–200-msec drift in the first Purkinje record, following each saccade, may be caused by a translation motion of the eye, inasmuch as a similar component is not seen in the fourth Purkinje record; (b), (c) comparing simultaneous horizontal and vertical overshoot components in the fourth Purkinje records with the subject relaxed to infinity and accommodated to 4 diopters. Note the large increase in overshoots at 4 diopters.

which shows the horizontal and vertical eye movement response to a diagonal target movement having 4° peak-to-peak components. In Fig. 17(b), the eye was relaxed to infinity, and in Fig. 17(c), the eye was accommodated to 4 diopters. At 4 diopters of accommodation, the limit for this subject, there is a large increase in the size and time constant of the overshoots in both the horizontal and vertical channels, as compared with relaxed accommodation. Still larger overshoots have been seen in subjects with larger accommodation. Note that the overshoots are not consistent from saccade to saccade, adding to the evidence that the overshoots are not in the instrument servoes. Also, the overshoots are generally larger in the horizontal than in the vertical direction for this subject.

If these overshoots derive from lateral motion of the lens within the globe, they provide a potentially useful method of measuring this motion. Also, such a motion causes a shift in the visual axis of the eye and, therefore, a shift in the retinal image. A large shift can have significant effects, for example, on the quality of image stabilization. We have estimated that the overshoots in the fourth Purkinje record are approximately ten times as large as the resulting shift in the visual axis, that is, a lateral shift of the lens large enough to cause a 1° overshoot in the fourth Purkinje record would actually represent about a 6-min shift in the visual axis of the eye.

If the magnitude of the overshoot could be scaled properly, the tracker would have an advantage in image stabilization over contact lens methods, which are insensitive to internal movements of the lens within the globe.

The stabilized image experiments referred to earlier⁸ were performed without compensating for these overshoots, implying that even better image stabilization might result from proper compensation of the overshoot signals to make them correspond to the actual image displacement.

F. Binocular Records

Figure 18 shows simultaneous 3-D recordings of both eyes. During this record, both eyes were stimulated by square wave accommodation stimuli of 2 diopters. The accommodation responses are shown in the records labeled A_L and A_R . During period A, both eyes saw a target that was stationary except for a change in optical distance, and the eyes were nominally stationary (that is, the accommodation response was not accompanied by the usual vergence response). During period B, the left eye was occluded; recordings then showed the familiar vergence movement in response to the accommodation change. The lower trace, labeled $H_R - H_L$, is the difference between the left and right horizontal channels and therefore measures vergence. During period C, both eyes again saw a fixed target.

During periods D and F, the targets in both eyes were made to move in a sinusoidal pattern horizontally and sawtooth pattern vertically. Note that the records during these periods are similar to those of Fig. 13, except that both eyes are recorded simultaneously. During period E, the left eye was again occluded, and the H_L channel shows that the left eye responds now with both the accommodation-driven vergence stimuli and the sine wave motion of the right (seeing) eye, driven by the yoked version response.

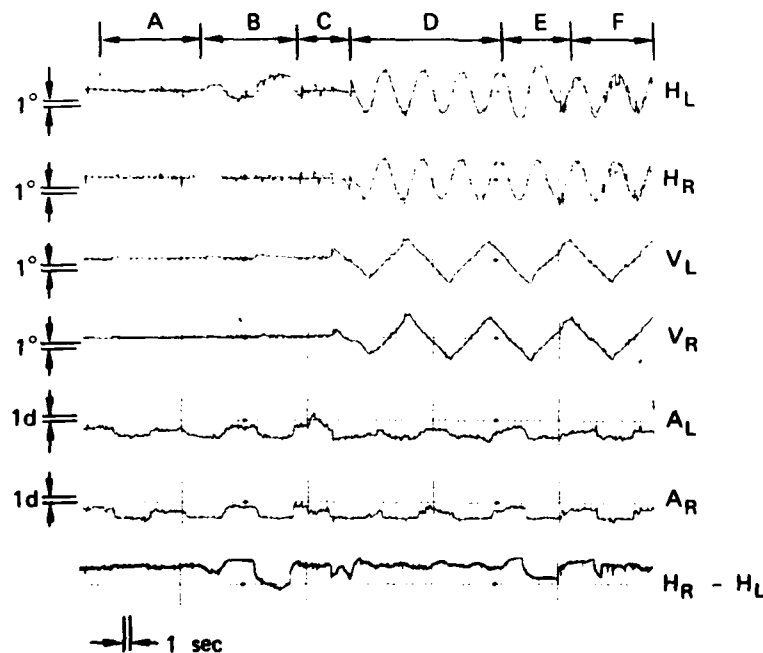


Fig. 18. 3-D, binocular record: H_L, H_R , horizontal motion in the left and right eye; V_L, V_R , vertical motion in left and right eye; A_L, A_R , accommodation in left and right eye; $H_R - H_L$, difference in horizontal motions in the two eyes (i.e., vergence) (see text for details).

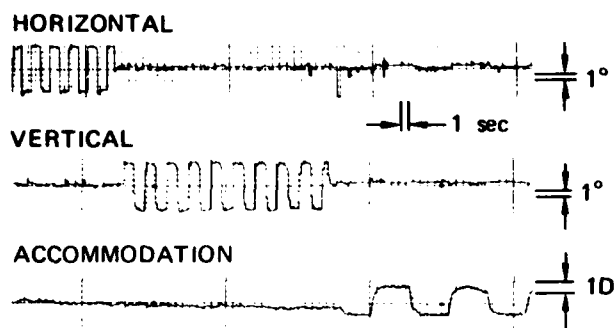


Fig. 19. Exploring channel interaction.

G. Channel Interaction

We have not yet studied in detail the effects of large eye movements on the calibration of the optometer and the effects of large accommodation changes on the calibration of the eyetracker. The records of Figs. 13 and 18 show that these effects are small, however, for ordinary eye movements and accommodation changes.

Nevertheless there are residual interactions. Figure 19 shows the 3-D response to a horizontal, then vertical, and then accommodation square-wave stimulus. There is almost no cross coupling into the other channels during the first two responses, although there is some coupling into the horizontal channel during the accommodation response. We do not yet know for sure how much of this coupling is in the eyetracker and/or stimulator and how much is in the eye, because there is some variation in cross coupling effects from subject to subject and even with the same subject from one session to another.

VII. Discussion

This instrumentation is relatively complex and operates on extremely low signal levels (especially the signals from the fourth Purkinje image of the 2-D eyetracker and from the retina in the optometer). Merging the two instruments, to achieve a 3-D tracker, required optical and electronic isolation measures so that the instruments would not interfere with each other. Furthermore, the latest version of the instrument is designed to tolerate head movements within 1 cm³ of space. This required developing a method of translating the input light beams (without any rotation components) and an automatic focus system (without any accompanying change in magnification), as discussed in connection with Fig. 4. The resulting 3-D instrument has high accuracy and good frequency response in all channels although there is a small amount of channel interaction—especially between horizontal eye movements and accommodation. There is also a very small amount of translation artifact present in the eye rotation records. With further study and evolution, we hope to be able to define the ultimate limits of this visual tracking technique.

VIII. Summary

We have described a 3-D eyetracker that simultaneously tracks the horizontal and vertical movements of the eye as well as its instantaneous refractive power. The instrument is a synthesis of two previously described instruments: a double-Purkinje-image eyetracker and an optometer. The light sources for both instruments are near ir (0.93 μ m) and are invisible to the subject. The eyetracker has a frequency response flat to approximately 300 Hz and operates over a field of more than 20° in diameter. The noise level of the eye-movement records is approximately 1 min of arc. Good stabilized-image disappearance has been achieved by moving the stimulus with the eyetracker output signals, which provides an indication of the accuracy and dynamic response of the instrument. The optometer operates over a range of 16 diopters with a noise level on the order of 0.1 diopter.

The instrument is easy to use; most new subjects can be aligned within a few minutes, and, once aligned, no adjustments are required as the subject moves in and out of the instrument. The instrument is designed to tolerate variations in head position within 1 cm³; signals indicating the 3-D position of the eye are also available.

A pair of 3-D eyetrackers, combined with a pair of 3-D visual stimulators, form the basis of a binocular system in which each eye can be stimulated in X, Y, and focus independently, while the 3-D eye movements are recorded simultaneously from both eyes.

The detailed optical design of the second-generation eyetracker portion of the 3-D instrument was mainly the work of R. E. Savoie. The authors are indebted to Michael Clark for his general help in the later stages of the development and in obtaining the records described in the section on performance.

The work of merging the optometer and the improved double-Purkinje-image eyetracker was supported by NIH grant EY 01031 from the Department of Health, Education, and Welfare.

References

1. T. N. Cornsweet and H. D. Crane, *J. Opt. Soc. Am.* **60**, 548 (1970).
2. T. N. Cornsweet and H. D. Crane, *J. Opt. Soc. Am.* **63**, 921 (1973).
3. It is important to understand that the fourth Purkinje system tracks the position of the fourth image relative to the first. Thus, although we may sometimes refer simply to the fourth Purkinje output, what is meant is the position of the fourth image with respect to, or relative to, the first.
4. In the first-generation instrument, the 90° reflection at mirror *M*, in Fig. 2, caused coupling of vertical eye motions into the horizontal measurement channel. With a vertical eye movement, mirror *M* rotates around axis *aa* (see inset in Fig. 2) to keep the first Purkinje image fixed on photocell *P*₁. This movement causes a rotation of the optical field around the first Purkinje image, producing artifactual change in the horizontal output for large eye movements. This problem is avoided in the new instrument by the 180° reflection at mirror *M*₁₀.

5. Experience with the first-generation eyetracker showed that a center-pivoted, 2-D mirror system is more accurate than a system that actually moves a photocell in two dimensions (i.e., photocell P_4 in Fig. 2). The new eyetracker therefore has two similar, 2-D servodriven mirror systems.
6. Isolation between instruments would be improved further if optometer light sources S_2 and S_3 emitted light of a different wavelength from that of eyetracker light source S_1 . The two instruments could then be isolated by optical filters. Light emitting diodes of different wavelengths bright enough for this application are just now becoming available.
7. H. D. Crane and M. Clark, this same issue.
8. D. H. Kelly, "New Method of Stabilizing Retinal Images," at annual meeting of Opt. Soc. Am., Boston, 21-24 October 1975.

Appendix B

THREE-DIMENSIONAL VISUAL STIMULUS DEFLECTOR

Reprinted from Applied Optics, Vol. 17, No. 5, pp. 706-714 (1 March 1978)

Three-dimensional visual stimulus deflector

H. D. Crane and Michael R. Clark

A 3-D visual stimulus deflector has been designed so that a subject can view any stimulus pattern or object through it, and the pattern (up to 25° in diameter) can be moved over a range of 40° horizontally and 30° vertically. The optical distance of the object being viewed can be changed over a 15-diopter range, while the brightness and visual angle subtended by the object remain fixed. Further, the observer can view the object through a pupil of any desired shape and transmittance. Horizontal and vertical movements are independent, with time delays of 1 msec and a response range from dc to 200 Hz. Focus change is independent of lateral field motion and has a time delay of 12 msec and a maximum slewing rate of approximately 40 diopters/sec. Two such devices can be aligned side by side in a binocular configuration for independent 3-D control of the fixation of each eye.

I. Introduction

To test the human visual system in a clinical or research setting, it is often necessary to move a target in specific ways to stimulate certain types of eye movements in the subject (patient). The instrument described here can move the visual stimulus horizontally and vertically, as well as stimulate accommodation (focus) by altering the optical distance of the target from the subject. The subject views the target through the deflector. Horizontal and vertical movements and focus change are accomplished with three independent servosystems. Independent, 3-D stimulation of both eyes is achieved by two devices aligned side by side.

The basic principle of operation may be summarized as follows (see Fig. 1). The subject's eye is positioned in front of the first lens pair LP_1 so that the center of rotation CR of the eye is imaged on the axis of rotation of mirror M_V . The two lenses of LP_1 are identical and separated by the sum of their focal lengths. This pair of identical lenses separated by the sum of their focal lengths produces an undistorted unity-magnification image. Mirror M_1 is fixed in position; mirror M_V is rotated by a closed-loop servomotor system to produce vertical movement of the visual field.

The eye is imaged a second time by lens pair LP_2 . Mirror M_H is positioned so that the eye's center of rotation in the second image falls on the axis of mirror

M_H . Mirror M_H is rotated by a second closed-loop servomotor system to produce horizontal movement of the visual field. With the axes of rotation of both mirrors conjugate to CR , pure horizontal and vertical movement of the visual field is achieved without either translation effects or image size changes.

The plane of the eye's pupil is conjugate to a plane labeled AP (artificial pupil). If a stop smaller than the natural pupil is placed in the artificial pupil plane, it becomes the limiting aperture of the system; consequently, the effects of natural pupil changes are eliminated. Cylindrical and spherical correction lenses for each subject can be placed in a trial lens holder located in front of aperture AP . Since plane AP is conjugate with the pupil of the eye, correction lenses placed near plane AP should have the same visual effect as if they were placed directly at the spectacle plane.

The second lens pair, LP_2 is positioned so that its first lens L_3 is located one focal distance from plane AP . Simultaneous axial movement of lens L_4 , mirror M_H (with its servomotor), and mirror M_2 adjusts the spherical power of the system without change in image position, size, or brightness. As we will show, spherical power, in diopters, is linearly related to the axial position of the movable carriage, which can be adjusted manually or driven by a third servomotor. Lenses L_1 , L_2 , L_3 , and L_4 are actually multiple-element camera lenses.

II. Theory of Operation

To understand the optics of the system, a discussion of certain properties of a pair of lenses separated by the sum of their focal lengths is necessary. The configuration used may be regarded as a relay-lens system.

The authors are with Stanford Research Institute, Menlo Park, California 94025.

Received 2 July 1977.

0003-6935/78/0301-0706\$01.50/0.

© 1978 Optical Society of America.

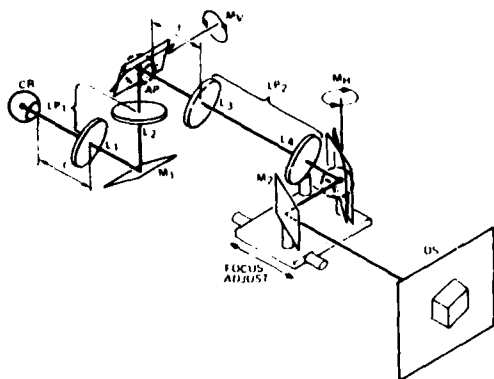


Fig. 1. Schematic diagram of the 3-D visual stimulator. CR, center of rotation of eye; L_1, L_2, L_3 , and L_4 , multiple-element camera lenses; LP, lens pair; AP, artificial pupil; DS, display screen; M_V , mirror that rotates the visual field vertically; M_H , mirror that rotates the visual field horizontally; M_1 , fixed mirror; L_4, M_H , and mirror M_2 move in synchronism to adjust the optical distance to the display screen (see Fig. 8).

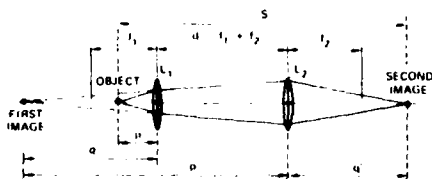


Fig. 2. Two-lens system. f_1, f_2 , focal lengths of lenses L_1, L_2 ; p , object distance to L_1 ; q , first image distance from L_1 ; p' , object distance from L_2 ; q' , second-image distance from L_2 ; d , separation between L_1 and L_2 ; S , separation between object and second image.

A. Linear Object-Image Motion

Figure 2 illustrates a pair of positive lenses of focal length f_1 and f_2 , separated by a distance d . An object at distance p from the first lens ($p < f_1$) forms an image at distance q' from the second lens.

It is well known that if $p = f_1$ then $q' = f_2$, independent of the separation d , and there is an image magnification $M = f_2/f_1$. Less well known is that when $d = f_1 + f_2$ (i.e., when the lenses are separated by the sum of their focal lengths), the distance p and q' are linearly related, and magnification M is independent of p .

For $p < f_1$ the image formed by L_1 , labeled the first image in Fig. 2, will be virtual and located at a distance

$$q = -pf_1/(p - f_1) \quad (1)$$

on the same side of the lens as the object. This first image is at a distance

$$p' = q + (f_1 + f_2) = \frac{pf_2 - f_1(f_1 + f_2)}{p - f_1} \quad (2)$$

from the second lens and forms a second image at a distance

$$q' = \frac{p'f_2}{p' - f_2} \quad (3)$$

from the second lens. Substituting Eq. (2) into Eq. (3) produces

$$q' = \left[f_2 \left(1 + \frac{f_2}{f_1} \right) \right] - \left(\frac{f_2}{f_1} \right)^2 p. \quad (4)$$

Thus the image distance q' is linearly related to the object distance p through the constant factor $(f_2/f_1)^2$. With $p = f_1$, Eq. (4) reduces to $q' = f_2$. It is straightforward to show that the same results are true for $p > f_1$.

The magnitude of the lateral magnification M between the object and final image can be determined from

$$M = \left| \frac{q}{p} \cdot \frac{q'}{p'} \right| = \left| \frac{-pf_1/(p - f_1) \cdot p'f_2/(p' - f_2)}{p \cdot p'} \right| \quad (5)$$

or

$$M = \left| \frac{-f_1 f_2}{(p - f_1)(p' - f_2)} \right|. \quad (6)$$

Substituting Eq. (2) for p' results in the simple equation

$$M = f_2/f_1, \quad (7)$$

which depends only on the ratio of the focal lengths and is independent of p .

Because axial image position is linearly related to object position and lateral image magnification is independent of object distance, axial magnification is uniform, and lateral magnification is constant in the image [see Fig. 3(a) for the case of $f_2/f_1 = 2$]. In this case, lateral magnification is two, and axial distances are scaled by $2^2 = 4$. Figure 3(b) shows the usual distortion that results from single lens imaging for the same magnification.

B. Object-Image Separation

The separation S between the object and the second image in Fig. 2 is

$$S = p + (f_1 + f_2) + q'. \quad (8)$$

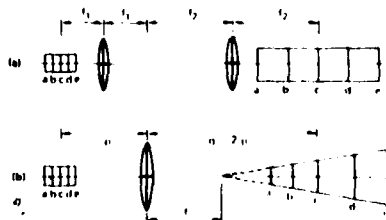


Fig. 3. (a) Relay lens pair. Lateral and axial magnification are independent of axial position of the object. Note the distortionless and constant imaging from (abcde) to (a'b'c'd'e'). (b) Typical distortion of single-lens imaging.

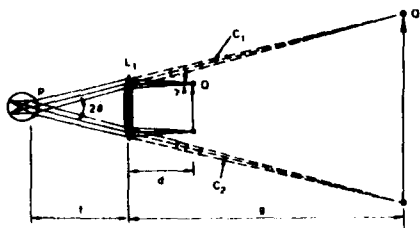


Fig. 4. Schematic representation of a simple Badel optometer. The pupil plane of the eye is placed one focal length f from lens L_1 ; the object, a distance d from L_1 , subtends a visual angle 2θ ; a virtual image of the object is formed at a distance g from L_1 ; note the backward projection of central rays C_1 and C_2 ; p , pupil diameter.

Substituting Eq. (4) for q' results in

$$S = p \left[1 - \left(\frac{f_2}{f_1} \right)^2 \right] + f_1 \left(1 + \frac{f_2}{f_1} \right)^2. \quad (9)$$

For $p = f_1$, Eq. (9) reduces to $2(f_1 + f_2)$. For $f_1 = f_2 = f$, the separation is constant and equal to

$$S = 4f, \quad (10)$$

independent of p . This result is expected once it is noted that, with equal-power lenses, image movement exactly tracks object movement. Alternatively, for a fixed object location, the lens pair itself can be moved without affecting the image position.

Even if there is a nonunity ratio, magnification will still remain constant although S varies linearly with p . Thus, if the spacing between the object plane and the desired image plane should change, either because the object moved or because the image screen moved, the system can be refocused by moving the lens pair along the optic axis. When refocused, the image will be unchanged in size because of the constant magnification property.

C. Basic Principle of Focus Corrector/Deflector

In the optical system sometimes referred to as a Badel optometer, the eye views an object through a lens that is located one focal length from the pupil of the eye, as illustrated in Fig. 4. (More specifically, the lens is placed one focal length from the first nodal point of the eye, which is approximately in the pupil plane of the eye.) The optical power of the system is adjusted by varying the distance d between the object and lens. Lens L_3 of Fig. 1, which is located one focal length from the first image of the pupil, is functionally equivalent to lens L_1 of Fig. 4. Movement of lens L_4 in Fig. 1 varies the distance d between the real image formed of the display screen DS and lens L_3 . Hence, L_3 functions as a Badel optometer that is separated from the eye by a relay lens pair LP_1 .

Viewing through lens L_1 of Fig. 4, the eye sees the object, located a distance d on the far side of the lens, imaged at a distance $f + g$ from the lens. As illustrated by Fig. 4,

$$1/g = 1/d - 1/f \quad (11)$$

or

$$g = (fd)/(f - d), \quad (12)$$

and therefore

$$f + g = f^2/(f - d). \quad (13)$$

The distance to the image in diopters D_E is

$$D_E = \frac{1}{f + g} = \frac{1}{f} \left(1 - \frac{d}{f} \right) = D_o \left(1 - \frac{d}{f} \right), \quad (14)$$

where f and g are measured in meters, and $D_o = 1/f$ is the dioptric power of the lens. If $d = f$, the object appears at infinity, and the relative power of the eye D_E required to focus the object is zero.¹ If $d = 0$, the lens has no optical effect, and the object appears to the eye at the distance of the lens. The accommodation power required to focus it is therefore $1/f$, or D_o , diopters. If $d > f$, the object appears beyond infinity, and the required eye power is negative. Note that the relationship expressed in Eq. (14) between eye diopters and distance d is linear.

The angular size of the object is independent of d because the backward projection of the central rays from each point of the object, for example, rays C_1 and C_2 from the two extreme points of the object are independent of d . Image brightness is also independent of d because the fan of rays accepted from each point of the object is independent of d . To see this, note that the fan of rays accepted at the pupil from object point Q has an angular extent γ as viewed from the object point. Using the small angle approximation, we have

$$\gamma = [pg/(f + g)]/d, \quad (15)$$

where p is the pupil diameter. Substituting Eq. (12) and Eq. (13) into Eq. (15) results in

$$\gamma = p/f, \quad (16)$$

which is independent of d . This result is true for every point of the object. For this reason, image brightness is independent of the focal power of the instrument.

Crane and Cornsweet devised a system, shown in Fig. 5, that does not require the object to be moved to change the virtual distance d .² An image of the object to be viewed is formed by a lens L_2 in the space between L_1 and L_2 . The distance from this real image to lens L_1 (distance d) is smoothly varied by means of a four-component mirror system. With the eye fixed in the focal plane of lens L_1 , an image of the eye pupil is formed in the focal plane to the right of lens L_2 . For this method of imaging, the light coming to focus at AP is collimated between the lenses, and the image of the eye pupil is therefore unaffected by movement of the mirrors. Hence, an artificial pupil AP can be used in this image plane.

D. Large Field of View

Using spherically corrected doublets, a system of the form shown in Fig. 5 can operate well over a viewing field up to about 10° . To increase the field of view, however, requires camera-quality optics.

To understand the optical requirements, let us sim-

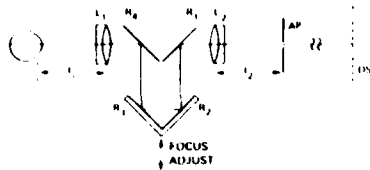


Fig. 5. Crane and Cornsweet focus stimulator: *DS*, display screen; *AP*, artificial-pupil plane. Mirrors R_2 and R_3 are moved orthogonal to the optic axis to change the optical distance to *DS*.

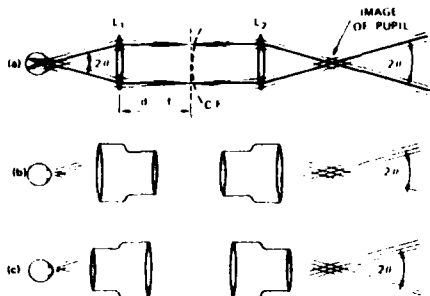


Fig. 6. (a) Schematic diagram of a relay lens pair with a visual field 2θ . The pupil plane of the eye is placed at the focal plane of L_1 . Assume the eye is focused at infinity, i.e., $d = f$. C.F. depicts curvature of field. (b) Camera-quality lenses arranged for minimal blurring of images at the retina. (c) Camera-quality lenses arranged to minimize spherical aberration.

plify the drawing by straightening out the path between the lenses of Fig. 5, as shown in Fig. 6(a), in which the eye is shown focused for infinity, and the image of display screen *DS* is also at infinity, i.e., $d = f$. In effect, the eye views the target through the entrance pupil formed by lenses L_1 and L_2 . There are two conflicting requirements for good imaging in this case. First, zero field distortion requires that the chief rays (shown dark in the figure) passing through the center of the real pupil should also intersect at the center of the pupil image. (In this case, the field angle, labeled 2θ , would be the same whether seen from the real pupil or from the pupil image.) This requires zero spherical aberration in the plane of the pupil. Second, note that a real image of the infinitely distant scene is formed in the plane between the two lenses. This real image serves, in turn, as the virtual object for lens L_1 . Any curvature of field in this image plane, as suggested by curved line C.F. in the figure, would cause off-axis blurring of the image at the retina. These requirements—zero spherical aberration and flat-field imaging—generally conflict for doublet lenses.

Camera lenses substituted for lenses L_1 and L_2 should be arranged as shown in Fig. 6(b) to minimize blurring of the target at the retina. That is, they should be arranged as though the plane between the two lenses is the normal film plane; camera lenses are specifically designed for flat-field imaging in this direction. On the

other hand, to minimize spherical aberration in imaging the eye pupil, the lenses should be reversed, as shown in Fig. 6(c). Recall that with respect to the pupil, the rays are collimated between the lenses. The design discussed here is based on a relatively symmetric 50-mm Olympus $f/1.8$ camera lens which can be used almost equally well in both directions, although configuration 6(c) provides a significantly wider field of view.

The difficulty with camera lenses, whether used in configuration 6(b) or 6(c), is that they are too large to use with the four-mirror scheme of Fig. 5. The only practical arrangement is to move the lens itself, as illustrated in Fig. 7(a). The disadvantage of moving the lens is that unless the display screen is at optical infinity, the distance from the screen to the lens is then variable, and the image formed between the lenses is no longer constant in size. The situation can be remedied with an extra fixed lens if the display screen can be placed directly in the focal plane of the extra lens. By using two extra lenses, L_3 and L_4 [as shown in Fig. 7(b), where L_4 generates a real image of the display screen in the focal plane of lens L_3], the system can then accommodate a continuous range of distances between the device and display screen. That is, for a given position of the display screen *DS*, lens L_4 is adjusted axially until image DS' is in the focal plane of lens L_3 . This places the image DS' of *DS* at infinity, making the image size independent of focus adjustments.

Two extra lenses are necessary, in any case, for achieving two-axis visual deflection as well as focus control. That is, two separate images of the eye pupil

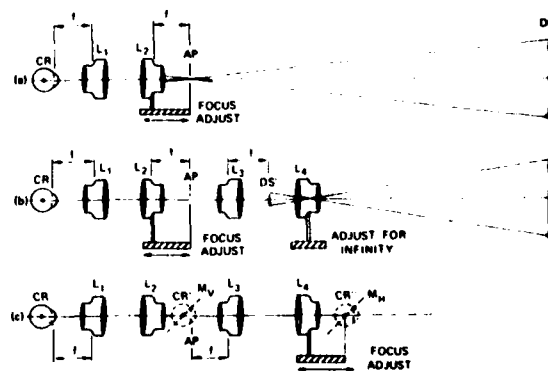


Fig. 7. (a) Simple focus stimulator. Lens L_2 moves axially to vary dioptric power; artificial pupil *AP* eliminates any effects caused by changes in the eye pupil; *DS*, display screen. (b) Focus stimulator that compensates for variable axial position of the display screen. L_4 is moved axially to create an image of *DS* in the focal plane of L_3 , thereby ensuring that the target *DS* appears at optical infinity to the focus stimulator system (L_1 , L_2). (c) Three-dimensional visual stimulator; M_V and M_H , rotating mirrors; *CR*, center of rotation of eye; CR' , CR'' , first and second images of *CR*. With CR' and CR'' on the axes of rotation of M_V and M_H , respectively, vertical and horizontal movement of the visual field is achieved without translation artifact.

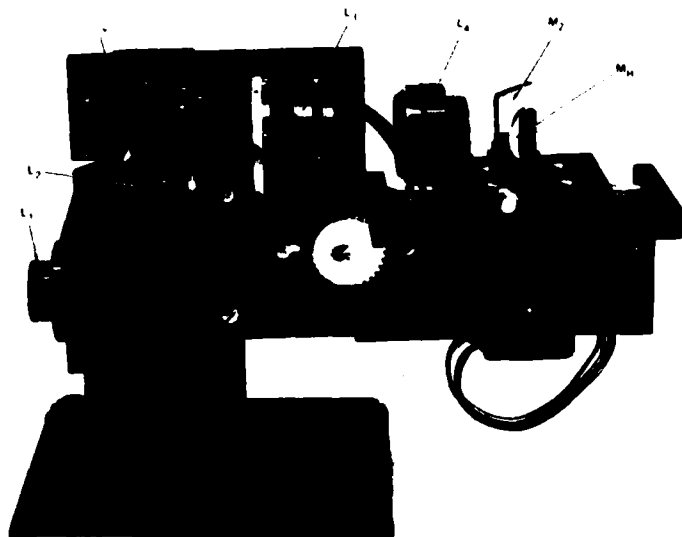


Fig. 8. Three-dimensional visual stimulator (see schematic diagram of Fig. 1).

are required as locations for two single-axis mirror deflectors, as illustrated in Fig. 1 and again in Fig. 7(c). Mirror M_V is positioned at the first image location (between the two lens pairs); mirror M_H is located at the second image location (beyond the second lens pair). It was noted earlier that to achieve pure rotation of the visual field without translation effects, it is necessary that the eye's center of rotation be conjugate to some point on the axis of rotation of each mirror. If lens L_2 were used for focus control, as shown in Fig. 7(b), both images of the eye's center of rotation would shift axially with respect to the mirror axes shown in Fig. 7(c), unless both servomotor mirror assemblies shifted axially by different amounts in synchronism with L_2 . The system is greatly simplified if lens L_4 is used instead for focus adjustment, in which case only mirror assembly M_H must be moved axially, as shown in Fig. 7(c).

With the position of Lens L_4 adjustable, the spacing between lenses L_3 and L_4 is no longer constant, and the imaging of the eye at mirror M_H is no longer distortionless as it would be if the distance between L_3 and L_4 were equal to the sum of their focal lengths. But only small errors result. Appendices A, B, and C analyze the magnitude of the errors inherent in the system.

III. Performance

Figure 8 shows the 3-D visual stimulator. The field of view is approximately 25° in diameter. The center of the field can be moved through an angle subtending $\pm 15^\circ$ vertically and/or $\pm 20^\circ$ horizontally at the eye. The spherical power can be changed from -4 diopters to $+11$ diopters with a movement sensitivity of 2.5 mm/diopter. Each camera lens has ten surfaces. The loss of light when viewing through the forty coated surfaces of four camera lenses in series is equivalent approximately to a 0.3 neutral density filter.

The electronics that produce horizontal and vertical deflections consist of the two General Scanning CCX-101 amplifiers that drive the G300PD Optical Scanners (see Fig. 9). The scanners have angular rotation sensors that are used to derive angle and angle rate signals that are part of a servo loop. A readout of the angular position of the scanners is available. Gain and offset controls condition the input signal while loop gain and damping adjustments are also available.

The deflection servosystems are capable of rotating the mirrors by more than 25° (50° movement of the visual target) with a linearity of $\pm 0.1\%$ of the excursion. The resolution is approximately 10 sec of arc with a response from dc to 3-dB bandwidth of 200 Hz. The delay time (0-10%) is less than 1.5 msec, and the 10-90 risetime is less than 2.5 msec. The total response time is approximately 6 msec.

The focus servo, a closed-loop system with position feedback, is capable of changing spherical power by more than 14 diopters with a sensitivity of approximately 9 diopter/V. The linearity is $\pm 0.25\%$ of the peak-to-peak range with a repeatability of less than 0.1 diopters. The time delay to a step is 12 msec with a maximum slewing rate of 40 diopter/sec.

IV. Summary

A 3-D visual stimulus deflector consists of four identical camera lenses in series. It is shown that a pair of identical lenses separated by the sum of their focal lengths generates an undistorted 3-D image independent of the distance that the object is from the lens pair. With two such pairs of lenses, two undistorted images are created, one in the space between the second and third lens and one in the focal plane beyond the fourth lens. The eye sees the world as though viewing through this second image of itself. A rotatable mirror is located at each of these image positions and adjusted so that the image of the eye's center of rotation falls on each axis of rotation. In this case, the field of view seen by the eye can be moved as though with a pure eye rotation, that is, without translational effects. A mirror that rotates about a horizontal axis is located at the first image position, and a mirror that rotates about a vertical axis is located at the second image position. These mirrors move the visual world in a vertical and horizontal direction.

Focus change is achieved by moving the fourth lens and second mirror in synchronism along the optical axis of the device. Although such movement alters the spacing between the third and fourth lenses (so they no

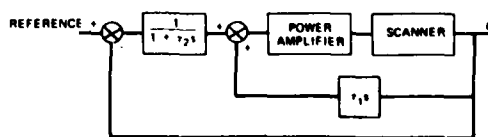


Fig. 9. Schematic diagram of deflection servoloop electronics.

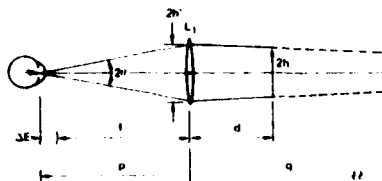


Fig. 10. Diagram of the change in visual angle as a function of object distance d from lens L_1 and axial misalignment of the eye by distance ΔE from the focal plane of L_1 .

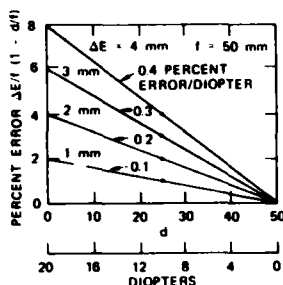


Fig. 11. Percent error in the visual angle θ as a function of the distance d of the object from lens L_1 ($f = 50$ mm).

longer form a distortionless imaging system) the errors thereby induced are small (see Appendices).

The instrument is built around four 50-mm $f/1.8$ camera lenses. It can move a visual stimulus 25° in diameter over a range of 40° horizontally and 30° vertically. The optical focus of the object being viewed can be changed over a 15-diopter range, while the brightness and visual angle subtended by the object remain invariant. Movement of the two mirrors and the axial movement of the last lens and second mirror system are controlled by three independent servosystems.

Appendix A

It was stated in the body of the paper in connection with Fig. 4 that if the eye is located in the focal plane of lens L_1 , the image size is independent of distance d . Let us inquire how sensitive this constancy is to the axial position of the eye.

Assume the eye is moved a distance ΔE from the focal plane, that is, the eye is at a distance $f + \Delta E$ from lens L_1 , and that the eye pupil is stopped down to a pinhole. In this case, the rays accepted from each point of the object will no longer be parallel, as shown in Fig. 4, but will converge as shown in Fig. 10. These accepted rays intersect at a distance q from the lens, where p and q can be thought of as object and image distances, that is,

$$q = \frac{pf}{p-f} = f \left(\frac{f+\Delta E}{\Delta E} \right). \quad (\text{A1})$$

The height $2h'$ of the accepted ray bundle at the lens can be written as

$$2h' = \frac{q}{q-d} \cdot 2h = \frac{1}{1-(d/q)} \cdot 2h, \quad (\text{A2})$$

where $2h$ is the object size. The angular size of the object, as seen from the eye, is

$$2\theta \approx (2h')/(f + \Delta E), \quad (\text{A3})$$

where the small-angle approximation is made that the angle is equal to its tangent. Substituting Eqs. (A1) and (A2) into Eq. (A3) gives the equation

$$\theta = \frac{h/f}{1 + \frac{\Delta E}{f} \left(1 - \frac{d}{f} \right)} \quad (\text{A4})$$

$$\approx \theta_0 \left[1 - \frac{\Delta E}{f} \left(1 - \frac{d}{f} \right) \right], \quad (\text{A5})$$

where the half angle $\theta_0 = h/f$.

Note that $\theta = \theta_0$ either if $\Delta E = 0$ (i.e., if the eye is in the focal plane) or if $d = f$ (i.e., if the object being viewed is at infinity). If $\Delta E \neq 0$, the image size will change as the object distance d changes. Figure 11 is a plot of the error factor $(\Delta E/f) [1 - (d/f)]$ for a 50-mm (20-diopter) lens. Note that according to Eq. (14) the eye will experience a 20-diopter change when the object shifts from $d = f$ to $d = 0$ (i.e., for a movement equal to f). The diopter change per millimeter of object movement can therefore be written

$$S = \frac{f}{1000/f} = \frac{f^2}{1000} \text{ mm/diopter} \quad (\text{A6})$$

or 2.5 mm/diopter for a 50-mm lens.

From Fig. 11, we see that with the eye displaced 2 mm axially, there is a 1% change in image size for a 6-diopter change (i.e., for a movement from $d = 50$ mm to $d = 35.0$ mm).

If the device is used as an ocular corrector, it is not important that the eye be in the exact axial plane because the target distance will not be changed. If the device is to stimulate focus change with constant image

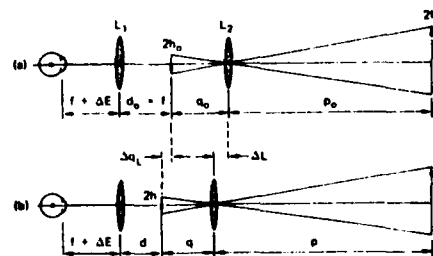


Fig. 12. Schematic representation of the axial shift ΔQ_L of an image because of a shift ΔL of L_2 . The eye is at a distance $f + \Delta E$ from L_1 . (a) Before lens movement, the object, height $2H$, is at a distance p_0 from L_2 and forms an image of height $2h_0$ at distance q_0 from L_2 and $d_0 = f$ from L_1 . (b) After lens movement ΔL , the object is at distance $p = p_0 + \Delta L$ from L_2 , and the image, height $2h$, is shifted by ΔQ_L to distance q from L_2 and d from L_1 .

size, however, alignment is important. The simplest way to adjust axial eye position is to move the eye axially slowly while the target shifts back and forth, until the subject reports no size change associated with the focus change. If the eye is too close to (or too far from) the lens, the target will increase (or decrease) in size as the target is brought toward the lens—i.e., decreasing d .

Appendix B

Figure 7 illustrates an axial lens shift to vary the focus. As we saw, however, unless the target is at infinity, this axial movement will cause a change in the size of the image. Also, the image will not move exactly the same amount as the lens movement. For the purpose of the following analysis, let Δq_L be the amount the image moves in response to a lens movement ΔL . The situation is shown in Fig. 12, where a deliberate axial shift of the eye is used to compensate for this variation in image size. In other words, focus change can be achieved while maintaining constant image size even with the target not at optical infinity. To obtain this result, we must find a value of ΔE such that θ (image size) is independent of d (distance).

Equation (A4) shows the general relation between θ , h , ΔE , and d , where the size of the real image being viewed $2h$ is now a variable. We will derive general relations for h and d as functions of ΔL .

By differentiating the general lens equation,

$$q = (pf)/(p - f), \quad (B1)$$

with respect to p , we find that for a small change Δp in object distance (lens fixed in position), the corresponding change in q is

$$\Delta q = -(q^2/p^2)\Delta p. \quad (B2)$$

If the object distance change is because of a shift ΔL in the lens, however, rather than because of a change in object position, the corresponding change in image position is simply equal to Δq plus the amount of the lens movement, i.e.,

$$\Delta q_L = \Delta L + \Delta q. \quad (B3)$$

Substituting Eq. (B2) into Eq. (B3) and noting that $\Delta p = \Delta L$, we obtain

$$\Delta q_L = \Delta L [1 - (q/p)^2]. \quad (B4)$$

In other words, if the lens moves by an amount ΔL to the left, the distance d decreases to

$$d = d_o - \Delta q_L \quad (B5)$$

$$= d_o - \Delta L [1 - (q/p)^2]. \quad (B6)$$

Let us consider next how image size varies with ΔL . The ratio of image size to object size is directly related to the ratio q/p , that is,

$$2h = (q/p) \cdot 2H, \quad (B7)$$

where q and p can be expressed as

$$p = p_o + \Delta p, \quad (B8)$$

$$q = q_o + \Delta q = q_o - (q/p)^2 \Delta p. \quad (B9)$$

Substituting Eqs. (B8) and (B9) into Eq. (B7), we obtain

$$h = h_o \frac{1 - \left[\left(\frac{q}{p} \right)^2 \cdot \frac{\Delta p}{q_o} \right]}{1 + \frac{\Delta p}{p_o}}, \quad (B10)$$

where $h_o = (q_o/p_o)H$. Ignoring second-order terms, Eq. (B10) becomes

$$h \approx h_o \left[1 - \frac{\Delta L}{p_o} \left(1 + \frac{q_o}{p_o} \right) \right], \quad (B11)$$

where ΔL is substituted for Δp . Substituting Eqs. (B6) and (B11) into Eq. (A4) and ignoring the subscripts on p , q , and d , we obtain

$$\theta \approx \frac{h_o}{f \left[1 + \frac{\Delta E}{f^2} (f - d) \right]} \cdot \frac{1 - \frac{\Delta L}{p} \left(1 + \frac{q}{p} \right)}{1 + \frac{\Delta E \Delta L \left(1 - \frac{q^2}{p^2} \right)}{f^2 + \Delta E (f - d)}}. \quad (B12)$$

Note that if the last terms of both the numerator and denominator are equal, Eq. (B12) reduces to

$$\theta \approx \frac{h_o}{f} \cdot \frac{1}{1 + [(\Delta E)/(f^2)](f - d)}, \quad (B13)$$

and θ is independent of ΔL , which is what we wished to demonstrate. The equality of numerator and denominator in Eq. (B12) requires that

$$\Delta E = \frac{-f^2}{(p - q) + (f - d)}. \quad (B14)$$

Figure 13 is a plot of Eq. (B14) for $f = d$, i.e., where the target appears to be at infinity, and therefore defines the initial ΔE for most experimental conditions. Note that ΔE is negative because as lens L_2 moves toward lens L_1 , the image decreases in size. To compensate for this decrease, the eye must be moved closer to lens L_1 . For example, for an object 1 m away ($p = 1000$ mm), the

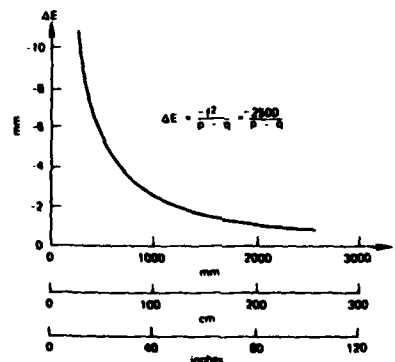


Fig. 13. Plot of ΔE as a function of the object distance p (from L_2) necessary to produce constant size imaging by lens system L_1, L_2 in Fig. 12. Note that $f = d$.

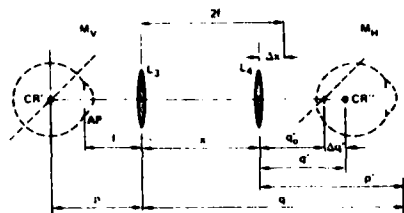


Fig. 14. Diagram of the axial movement $\Delta q'$ of the second image CR'' of the eye's center of rotation CR as a function of (L_4, M_H) movement by amount Δx . Before movement, Δx is zero and $x = 2f$; CR'' is at a distance q_0 from L_4 and falls on the axis of rotation of M_H . After movement, CR'' is displaced by $\Delta q'$ from the axis of rotation of M_H . The first image CR' of CR is formed at the axis of rotation of M_V , which is at a fixed distance p from L_3 . An image of CR' is formed at distance q' from L_4 .

eye must be moved approximately 2.5 mm closer to L_1 . Note that there is a very small sensitivity to the exact slide position before it is moved. For example, for $p = 1000$ mm, there is approximately a 1.3% change in ΔE for $d_0 = f$ (the slide at the infinity position) or for $d_0 = 3/4f$ (the slide at the 5-diopter position).

Appendix C

Even if mirror M_H moves in synchronism with lens L_4 , as illustrated in Fig. 7(c), the second image CR'' of the eye's center of rotation moves away from the surface of mirror M_H as lens L_4 moves over its range, as shown in Fig. 14. Therefore, rotation of M_H will not be perceived as pure rotation by the eye. The following discussion quantifies the expected variation of the translation component thereby induced.

Figure 14 depicts the geometry of interest. CR' , the image of CR formed at M_V , is at a distance p from L_3 .³ Its image distance q may be written

$$q = (pf)/(p - f). \quad (C1)$$

The object distance p' for lens L_4 can be written

$$p' = x - q = x - [(pf)/(p - f)] \leq 0, \quad (C2)$$

where x is the separation between lenses L_3 and L_4 . The separation x can in turn be written as

$$x = 2f + \Delta x, \quad (C3)$$

where Δx (positive or negative) represents the simultaneous movement of L_4 and M_H , as shown in Fig. 7(c). Substituting Eqs. (C1) and (C3) into Eq. (C2), we have

$$p' = \frac{pf - 2f^2}{p - f} + \Delta x. \quad (C4)$$

For simplicity, if we assume $p = kf$, $k > 1$, then Eq. (C4) becomes

$$p' = [(k - 2)/(k - 1)]f + \Delta x. \quad (C5)$$

The final image distance q' is

$$q' = \frac{p'f}{p' - f} = \frac{[(k - 2)/(k - 1)]f^2 + (\Delta x)f}{[(-f)/(k - 1)] + \Delta x}. \quad (C6)$$

Dividing the numerator by the denominator, we have

$$\begin{aligned} q' &= f + (1 - k)f / \left[1 - \frac{(k - 1)}{f} \Delta x \right] \\ &\approx f + [(1 - k)f] \left[1 + \frac{(k - 1)}{f} \Delta x \right] \\ &\approx (2 - k)f - (k - 1)^2 \Delta x. \end{aligned} \quad (C7)$$

Writing q' in the form

$$q' = q_0' + \Delta q' = q_0' \left(1 + \frac{\Delta q'}{q_0'} \right) \quad (C8)$$

and substituting Eq. (C7) into Eq. (C8), we have

$$q_0' = (2 - k)f, \quad (C9)$$

$$\frac{\Delta q'}{q_0'} = - \frac{(k - 1)^2}{2 - k} \frac{\Delta x}{f}. \quad (C10)$$

Figure 15 is a plot of $|\Delta q'|/(q_0')$ as a function of $(\Delta x)/f$, assuming $k = 1.2$. The maximum variation is 2.5% of q_0' in the worst case. This error will cause the conjugate image of the center of rotation to be displaced by this amount from the axis of the rotating mirror M_H . Consequently, the rotation of the eye caused by a given angular rotation of the mirror will not be exactly the same as the mirror rotation, or conversely, the rotation of the mirror necessary to compensate a given eye rotation will not be exactly the same size as the eye rotation.

The rotational error is depicted in highly exaggerated form in Fig. 16, where for simplicity the target is shown along the axis rather than as deflected by mirror M_H (i.e., as though M_H were not there). If M_H caused the

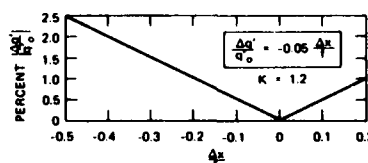


Fig. 15. Percent error $|\Delta q'|/(q_0')$ as function of the change in axial separation $(\Delta x)/f$ of L_3, L_4 .

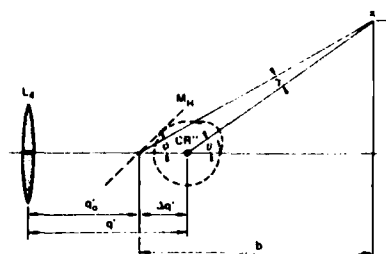


Fig. 16. Schematic diagram of the difference between rotational angle ϕ and visual angle θ , where the target is at a distance b from the axis of rotation of M_H and where the axis of rotation of M_H and CR'' are separated by a distance $\Delta q'$.

target to be rotated through an angle ϕ , the eye must rotate through an angle θ , where ϕ and θ differ by an amount

$$\gamma = \theta - \phi \quad (C11)$$

because of the offset $\Delta q'$. These angles can be written as

$$\phi = \tan^{-1}(a/b), \quad (C12)$$

$$\theta = \tan^{-1}[a/(b - \Delta q')], \quad (C13)$$

where b is the target distance from the axis of the mirror, which is approximately 1 cm larger than the distance from (the image of) the pupil to the target. For the present applications,

$$\phi \leq 10^\circ \quad (C14)$$

and

$$b > 10 \text{ cm } (D_E < 10 \text{ diopters}). \quad (C15)$$

Therefore,

$$a \leq b \tan 10^\circ = 0.176b. \quad (C16)$$

From Eqs. (C9) and (C10), it can be noted that

$$|\Delta q'| = (k - 1)^2 \Delta x. \quad (C17)$$

In the present design, $k = 1.2$ and $\Delta x \leq f/2$. Given $f = 50 \text{ mm}$, then $b > 2f = 10 \text{ cm}$. When we combine these relationships, Eq. (C17) becomes

$$|\Delta q'| = 0.04 \Delta x \leq 0.02f \leq 0.01b, \quad (C18)$$

$$\theta \leq \tan^{-1}(0.176/0.99) = 10.1^\circ, \quad (C19)$$

$$\gamma = \theta - \phi \leq 0.1^\circ. \quad (C20)$$

Thus, in the worst case, there is an (0.1/10) or 1% error between actual eye rotation and rotation of M_H because of the movement of lens L_4 .

If ϕ and the dioptric power [$D_E = (1/b)$] are constant, the gain of the servo driving M_H can be changed to overcome this artifact, since the correction factor is a constant. Also if $\phi \approx 0$ or $D_E \leq 0$, this error is negligible. Finally, if the error is noticeable and the position of L_4 is fixed ($D_E = \text{constant}$), $\Delta q'$ might be reduced to zero by locating the mirror M_H at a distance q' from L_4 .

This development was supported by grant 1 R01 EY01031 from the Department of Health, Education, and Welfare. The authors acknowledge the contributions of Lloyd Alterton and Carroll Steele of Stanford Research Institute to the mechanical and electronic design.

References

1. We use the convention, here, of stating refractive power of the eye relative to its power when accommodated for infinity, that is, 0.0 diopters of refractive power means that the retina is conjugate with infinity, at 2.0 diopters, the retina is conjugate with a plane 1/2.0 m away, etc. The absolute refractive power of a normal eye accommodated for infinity is about 60 diopters (i.e., its equivalent focal length is about 17 mm).
2. H. D. Crane, and T. N. Cornsweet, J. Opt. Soc. Am. 60, 577 (1970).
3. The position of CR' is determined by the fact that the image of the eye pupil must be located in the focal plane of L_3 to ensure constancy of brightness and image size independent of the position of L_4 .